図4　RNaseH 変異は核酸結合領域とは異なる外側に集積している

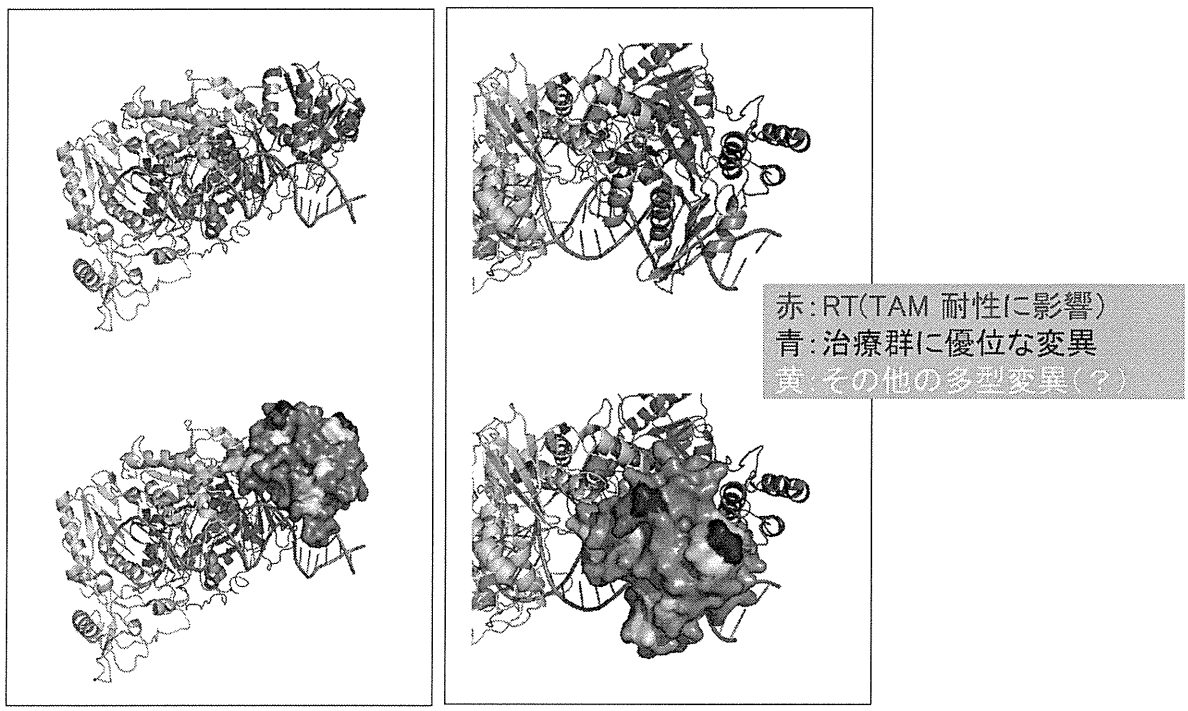

図１７：RNase H 領域の遺伝子変異の分布

研究成果の刊行に関する一覧表

雑誌

発表者氏名	論文タイトル	発表誌名	巻号	ページ	出版年
Matsuyama S., Aydan A., Ode H., Hata M., Sugiura W., Hoshino T.	Structural and Energetic Analysis on the Complexes of Clinically-isolated Subtype C HIV-1 Proteases and Approved Inhibitors by Molecular Dynamics Simulation	J. Phys. Chem. B	114 (1)	521-530	2010
Yanagita H., Urano E., Matsumoto K., Ichikawa R., Takaesu Y., Ogata M., Murakami T., Wu H., Chiba J., Komano J., Hoshino T.	Structural and Biochemical Study on the Inhibitory Activity of Derivatives of 5-nitro-furan-2-carboxylic acid for RNase H Function of HIV-1 Reverse Transcriptase	Bioorg. Med. Chem.	19	816-825	2011
Yanagita H., Yamamoto N., Fuji H., Liu X., Ogata M., Yokota M., Takaku H., Hasegawa H., Odagiri T., Tashiro M., Hoshino T.	Mechanism of drug resistance of hemagglutinin of influenza virus and potent scaffolds inhibiting its function	ACS Chem. Biol.	**7** (3)	552-562	2012
Yanagita H., Fudo S., Urano E., Ichikawa R., Ogata M., Yokota M., Murakami T., Wu H., Chiba J., Komano J., Hoshino T.	Structural Modulation Study of Inhibitory Compounds for RNase H Activity of HIV-1 Reverse Transcriptase	Chem. Pharm. Bull.	60 (6)	in press	2012
Hassan R., Suzu S., Hiyoshi M., Takahashi-Makise N., Ueno T., Agatsuma T., Akari H., Komano J., Takebe Y., Motoyoshi K., Okada S.	Dys-regulated activation of a Src tyroine kinase Hck at the Golgi disturbs *N*-glycosylation of a cytokine receptor Fms	J. Cell Physiol.	221(2)	458-468	2009
Urano E., Ichikawa R., Morikawa Y., Yoshida T., Koyanagi T., Komano J.	T cell-based functional cDNA library screening identified SEC14-like 1a carboxy-terminal domain as a negative regulator of human immunodeficiency virus replication	Vaccine	28S	B68-B74	2010

Kariya Y., Hamatake M., Urano E., Yoshiyama H., Shimizu N., Komano J.	Dominant-negative derivative of EBNA1 represses EBNA1-mediated transforming gene expression during the acute phase of Epstein-Barr virus infection independent of rapid loss of viral genome	Cancer Sci.	101 (4)	876-881	2010
Suzuki S., Maddali K., Hashimoto C., Urano E., Ohashi N., Tanaka T., Ozaki T., Arai H., Tsutsumi H., Narumi T., Nomura W., Yamamoto Y., Pommier Y., Komano J.A., Tamamura T.	Peptidic HIV integrase inhibitors derived from HIV gene products: structure-activity relationship studies	Bioorg. Med. Chem.	18 (18)	6771 - 6775	2010
Suzuki S., Urano E., Hashimoto C., Tsutsumi H., Nakahara T., Tanaka T., Nakanishi Y., Maddali K., Han Y., Hamatake M., Miyauchi K., Pommier Y., Beutler J.A., Sugiura W., Fuji H., Hoshino T., Itotani K., Nomura W., Narumi T., Yamamoto N., Komano J.A., Tamamura H.	Peptide HIV-1 integrase inhibitors from HIV-1 gene products	J. Med. Chem.	53 (14)	5356 - 5360	2010
Aoki T., Shimizu S., Urano E., Futahashi Y., Hamatake M., Tamamura H., Terashima K., Murakami T., Yamamoto N., Komano J.	Improvement of lentiviral vector-mediated gene transduction by genetic engineering of the structural protein Pr55Gag	Gene Therapy.	17 (9)	1124 - 1133	2010
Hamatake M., Komano J., Urano E., Maeda F., Nagatsuka Y., Takekoshi M.	Inhibition of HIV replication by a CD4-reactive Fab of an IgM clone isolated from a healthy HIV seronegative individual	Euro J. Immunol.	40 (5)	1504 - 1509	2010
Urano E., Kuramochi N., Tomoda H., Takebe Y., Miyauchi K., Komano J., Morikawa Y.	Novel Postentry Inhibitor of Human Immunodeficiency Virus Type 1 Replication Screened by Yeast Membrane-associated Two-hybrid System	Antimicrob. Agents Chemother.	55 (9)	4251 - 4260	2011
Aoki T., Miyauchi K., Urano E., Ichikawa R., Komano J.	Protein transduction by pseudotyped lentivirus-like nanoparticles	Gene Ther.	18 (9)	936-941	2011

Takizawa M., Miyauchi K., Urano E., Kusagawa S., Kitamura K., Naganawa S., Murakami T., Honda M., Yamamoto N., Komano J.	Regulation of the susceptibility of HIV-1 to a neutralizing antibody KD-247 by non-epitope mutations distant from its epitope	AIDS.	in press	in press	2012
Nomura W., Hashimoto C., Ohya A., Miyauchi K., Urano E., Tanaka T., Narumi T., Nakahara T., Komano J., Yamamoto N., Tamamura H.	Synthetic C34 Trimer of HIV-1 gp41 Shows Significant Increase of Inhibition Potency	Chem. Med. Chem.	in press	in press	2012
Watanabe T., Urano E., Miyauchi K., Ichikawa R., Hamatake M., Misawa N., Sato K., Ebina H., Koyanagi Y., Komano J.	The hematopoietic cell-specific Rho GTPase inhibitor ARHGDIB/D4GDI limits HIV-1 replication	AIDS Res. Hum. Retroviruses.	in press	in press	2012
Imadome K., Yajima M., Arai A., Nakagawa-Nakagawa A., Kawano F., Ichikawa S., Shimizu N., Yamamoto N., Morio T., Ohga S., Nakamura H., Ito M., Miura O., Komano J., Fujiwara S.	CD4-positive T cells have a critical role in the proliferation of EBV-infected T and NK cells	PLOS Pathog.	in press	in press	2012
Iwatani Y., Chan D. S. B., Liu L., Yoshii H., Shibata J., Yamamoto N., Levin J. G., Gronenborn A. M., Sugiura W.	HIV-1 Vif-mediated ubiquitination/degradation of APOBEC3G involves four critical lysine residues in its C-terminal domain	Proc. Natl. Acad. Sci. USA	106	19539 - 19544	2009
Iwatani Y.	Study on molecular mechanism of host defense factor, APOBEC3G, against HIV	J. AIDS Research	11	218-222	2009
Fujisaki S., Yokomaku Y., Shiino T., Koibuchi T., Hattori J., Ibe S., Iwatani Y., Iwamoto A., Shirasaka T., Hamaguchi M., Sugiura W.	Outbreak of Infections by Hepatitis B Virus Genotype A and Transmission of Genetic Drug Resistance in Patients Coinfected with HIV-1 in Japan	J. Clin. Microbiol.	49	1017 - 1024	2010
Ibe S., Yokomaku Y., Shiino T., Tanaka R., Hattori J., Fujisaki S., Iwatani Y., Mamiya N., Utsumi M, Kato S., Hamaguchi M., Sugiura W.	HIV-2 CRF01_AB: first circulating recombinant form of HIV-2	J. Acquir. Immune. Defic. Syndr.	54	241-247	2010
松下修三、横山勝、宮内浩典、松田善衛、俣野哲朗、岩谷靖雅	HIV 細胞進入とその防御機序	日本エイズ学会誌	12	67-73	2010

Shibata J., Sugiura W., Ode H., Iwatani Y., Sato H., Tsang H., Matsuda M., Hasegawa N., Ren F., Tanaka H.	Within-host co-evolution of Gag P453L and protease D30N/N88D demonstrates virological advantage in a highly protease inhibitor-exposed HIV-1 case	Antiviral Res.	90	33-41	2011
Kitamura S., Ode H., Iwatani, Y.	Structural features of antiviral APOBEC3 proteins are linked to their functional activities	Frontiers in Microbiol.	2	258	2011
Li J., Hakata Y., Takeda E., Liu Q., Iwatani Y., Kozak CA., Miyazawa M.	Two genetic determinants acquired late in Mus evolution regulate the inclusion of exon5, which alters mouse APOBEC3 translation efficiency	PLoS Pathogens	8	E100247 8	2012
Murakami T, Kumakura S, Yamazaki T, Tanaka R, Hamatake M, Okuma K, Huang W, Toma J, Komano J, Yanaka M, Tanaka Y, Yamamoto N.	The Novel CXCR4 Antagonist, KRH-3955 Is an Orally Bioavailable and Extremely Potent Inhibitor of Human Immunodeficiency Virus Type 1 Infection: Comparative Studies with AMD3100	Antimicro. Agents. Chemother.	53 (7)	2940 - 2948	2009
Iwasaki, Y., Akari H., Murakami T., Kumakura S., Dewan Z., Yanaka M., Yamamoto N.	Efficient inhibition of SDF-1a-mediated chemotaxis and HIV-1 infection by novel CXCR4 antagonists.	Cancer Sci.	100	778-781	2009
村上 努	HIV 複製を制御する宿主因子の探索	J. AIDS Research	11 (3)	205-209	2009
村上 努	HIV の粒子形成のメカニズム—Gag蛋白に関する最新の知見—	Confrontin g HIV2009	35	5-7	2009
Murakami, T., Yamamoto N.	The role of CXCR4 in HIV infection and its potential as a therapeutic target (Review)	Future Microbiol ogy	5 (7)	1025 - 1039	2010
Nakahara T., Nomura W., Ohba K., Ohya A., Tanaka T., Hashimoto C., Narumi T., Murakami T., Yamamoto N., Tamamura H.	Remodeling of Dynamic Structures of HIV-1 Envelope Proteins Leads to Synthetic Antigen Molecules Inducing Neutralizing Antibodies	Bioconjug ate Chem.	21 (4)	709-714	2010

Tanaka T., Narumi T., Ozaki T., Sohma A., Ohashi N., Hashimoto C., Itotani K., Nomura W., Murakami T., Yamamoto N., Tamamura H.	Azamacrocyclic-metal complexes as CXCR4 antagonists.Azamacrocyclic-metal complexes as CXCR4 antagonists.	Chem. Med. Chem.	6	834-839	2011
Narumi T., Komoriya M., Hashimoto C., Wu H., Nomura W., Suzuki S., Tanaka T., Chiba J., Yamamoto N., Murakami T., Tamamura H.	Conjugation of cell-penetrating peptides leads to identification of anti-HIV peptides from matrix proteins.	Bioorg. Med. Chem.	20	1468 - 1474	2012
Harada M., Murakami H., Okawa A., Okimoto N., Hiraoka S., Nakahara T., Akasaka R., Shiraishi Y., Futatsugi N., Mizutani-Koseki Y., Kuroiwa A., Shirouzu M., Yokoyama S., Taiji M., Iseki S., Ornitz D.M., Koseki H.	FGF9 monomer-dimer equilibrium regulates extracellular matrix affinity and tissue diffusion	Nat Genet.	41(3)	289-298	2009
Okimoto N., Futatsugi N., Fuji H., Suenaga A., Morimoto G., Yanai R., Ohno Y., Narumi T., Taiji M.	High-performance drug discovery: computational screening by combining docking and molecular dynamics simulations	PLoS Comput. Biol.	5(10)	e1000528	2009
Watanabe H., Tanaka S., Okimoto N., Hasegawa A., Taiji M., Tanida Y., Mitsui T., Katsuyama M., Fujitani H.	Comparison of binding affinity evaluations for FKBP ligands with state-of-the-art computational methods: FMO, QM/MM, MM-PB/SA and MP-CAFEE approaches	Chem-Bio Inform. J.	10	32-34	2010
Taiji M., Okimoto N.	高性能計算による薬剤分子設計	日本化学会情報化学部会誌	29	55-60	2011
Kondo H., Okimoto N., Morimoto G., Taiji M.	Free-Energy Landscapes of Protein Domain Movements upon Ligand Binding	J. Phys. Chem. B	115	7629 - 7636	2011

Structural and Energetic Analysis on the Complexes of Clinically Isolated Subtype C HIV-1 Proteases and Approved Inhibitors by Molecular Dynamics Simulation

Shou Matsuyama,[†] Ay Aydan,[†] Hirotaka Ode,[†] Masayuki Hata,[‡] Wataru Sugiura,[§,∥] and Tyuji Hoshino*[,†]

Graduate School of Pharmaceutical Sciences, Chiba University, 1-33 Yayoi-cho, Inage-ku, Chiba 263-8522, Japan, College of Pharmaceutical Sciences, Matsuyama University, 4-2 Bunkyo-cho, Matsuyama 790-8578, Japan, AIDS Research Center, National Institute of Infectious Diseases, 4-7-1 Gakuen, Musashimurayama, Tokyo 208-1011, Japan, and Clinical Research Center, Nagoya Medical Center, 4-1-1 Sannomaru, naka-ku, Nagoya 460-0001, Japan

Received: August 28, 2009; Revised Manuscript Received: October 14, 2009

HIV-1 has a large genetic diversity. Subtype B HIV-1 is commonly found in patients in developed countries. In contrast, an increasing number of patients are infected with the non-B subtype viruses, especially with subtype C HIV-1, in developing countries. It remains to be clarified how mutations or polymorphisms in non-B subtype HIV-1 influence the efficacy of the approved inhibitors. In this study, we have performed molecular dynamics simulations on clinically isolated subtype C HIV-1 proteases in complex with three kinds of approved inhibitors. From the structural and energetic viewpoints, we identified the polymorphisms influencing on the binding of the inhibitors. The effect of the V82I mutation on the association with chemicals and the reason for rare appearance of the D30N mutation in subtype C HIV-1 were discussed in terms of the change of geometry of the residues in HIV-1 protease.

Introduction

Total number of patients infected with human immunodeficiency virus (HIV) is supposed to be 3.3 million in the world in 2007 and HIV infectious disease is still one of the serious threats to human beings.[1] HIV is separated into two types, HIV-1 and HIV-2, and most of the patients in the world carry HIV-1. According to its high genetic diversity, HIV-1 is classified into three groups, M (Main), O (Outlier), and N (non-M/non-O). Viruses in group M are further divided into nine subtypes and several circulating recombinant forms (CRFs). Among nine subtypes, subtype B HIV-1 is major in developed countries in North America and Europe. In contrast, the viruses other than subtype B, so-called non-B subtype HIV-1, are mainly found among patients in developing countries in Africa and South East Asia. Over half of the patients are infected with subtype C HIV-1 in the world.

HIV-1 has a gene coding the viral enzyme called HIV-1 protease (HIV-1 PR).[2] Since the inhibition of the action of this enzyme leads no maturation of viral precursor and incomplete replication of the virus,[3] the inhibitors against HIV-1 PR have been prescribed in the chemotherapy for HIV-1 infectious disease.[4−12] All the PR inhibitors released so far were mainly developed against subtype B HIV-1 PR. HIV-1 PR has a formation of homodimer and each monomer consists of 99 amino residues (Figure 1A). Polymorphisms are frequently observed in HIV-1 PRs.[13] For example, the K20I mutation dominantly appears in the PRs of subtype G and CRF02_AG, M36I appears in PRs of subtypes A, C, D, F, G, CRF01_AE, and CRF02_AG, V82I appears in subtype G, and I93L appears in subtype C. These polymorphisms are closely related to the difference in mutational pathways leading to emergence of the drug resistant variants among subtypes. As some epidemiological studies suggested, the polymorphisms in PRs will change drug efficacy among different subtypes.[14−24] It is interesting to note that some mutations such as D30N, which is known for the primary mutation for drug resistance in subtype B PR, are rarely seen in non-B subtype PRs.[18,25,26] A study based on the clinical data with hundreds of the subtype C- and subtype B-infected patients clearly suggested that a difference was observed in frequency of the D30N mutation between subtypes C and B, while little difference was seen for the L90 M mutation.[25] Further, significant differences were found in the rates of appearance of M36I, L63P, A71 V, V77I, and I93L between subtypes C and B. Hence, the difference in polymorphism between subtypes should be seriously considered for planning the chemotherapeutic protocol for the nonsubtype B-infected patients. Accordingly, the accumulation of the knowledge on the susceptibility of inhibitors or the emergence rate of drug resistant mutations is required for non-B subtype HIV-1.

In this study, we have performed molecular dynamics (MD) simulation on the complexes of clinically isolated subtype C HIV-1 PRs and its inhibitors. Three kinds of HIV-1 PRs are examined; two of them were isolated from patients who have no experience on the treatment with PR inhibitors, and one was isolated from a patient who failed in the therapy with one of the PR inhibitors; nelfinavir (NFV), because of the appearance of drug resistant mutations (Figure 1B, and Figure S1 and Table S1 in Supporting Information). Three kinds of inhibitors: atazanavir (ATV), nelfinavir (NFV) and saquinavir (SQV), have been examined through the present computational study (Figure 1C).

Additional MD simulations have been performed on the complexes of the subtype B HIV-1 PR and the inhibitors

* To whom correspondence should be addressed. Tel: +81-43-290-2926. Fax: +81-43-290-2925. E-mail: hoshino@faculty.chiba-u.jp.
[†] Chiba University.
[‡] Matsuyama University.
[§] National Institute of Infectious Diseases.
[∥] Nagoya Medical Center.

10.1021/jp908314f
Published on Web 11/06/2009

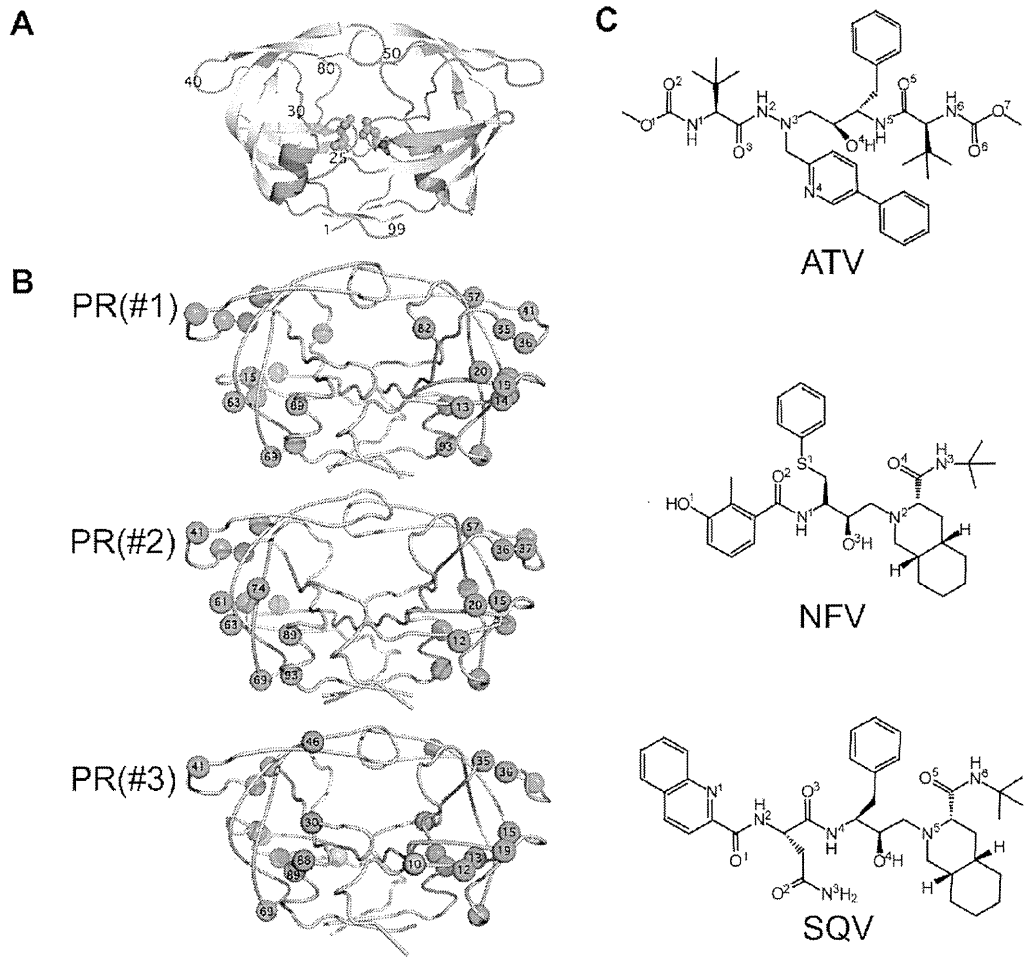

Figure 1. (A) Structure of HIV-1 PR. Locations of two catalytic aspartates are shown in the ball and stick representation. (B) Clinically isolated subtype C HIV-1 PR: PR(#1), PR(#2), and PR(#3). The red spheres indicate the D30N, M46L, and N88D mutations that are the primary mutations causing resistance to NFV. The orange sphere represents L10F, the secondary mutation to NFV. The green spheres represent the natural polymorphism seen in subtype C HIV-1 PR, differentiated from subtype B HIV-1 PR. The coloring of the spheres is based on HIVdb in Stanford University.[23] (C) Chemical structures of ATV, NFV, SQV.

introducing a single amino mutation. The aim of these calculations is to examine the difference in binding affinity or binding structure with the inhibitors between subtype B and subtype C HIV-1 PRs, and to clarify the change in mechanism for conferring drug resistance from the structural viewpoint. We particularly focus on (i) the role of the V82I mutation that is a common polymorphism seen in non-B subtype HIV-1 PR, and (ii) the effect of the D30N mutation in subtype C HIV-1 PR. Since subtype C HIV-1 PR has not sufficiently been surveyed in terms of the susceptibility for approved inhibitors and the emergence probability of drug resistant mutations, the information obtained in this study will give a hint to select the proper inhibitors for patients infected with subtype C HIV-1 and be helpful for the therapy for HIV-1 infectious disease in developing countries.

Methods

Molecular Dynamics (MD) Simulations. Minimizations and MD simulations were carried out using the Sander module of AMBER8.[27] The AMBER ff03 force field[28] was used as the parameters for proteins, ions, and water molecules. The general AMBER force field[29] was used as the parameters for ATV, NFV, and SQV. Our originally developed torsion parameters for the benzamide moiety in NFV, CA-CA-C -N and CA-CA-C -O, were applied.[30] Atom charges of inhibitors were determined from the electrostatic potential obtained from quantum chemical calculations, followed by the restrained electrostatic potential (RESP) fitting.[31] The stable structure of each inhibitor was determined through the geometry optimization at the HF/6-31G(d,p) level and, subsequently, the electrostatic potential was calculated at the B3LYP/cc-pVTZ level under the ether-phase condition. The quantum chemical calculations were executed with Gaussian03 program.[32]

We performed simulations of three clinically isolated subtype C HIV-1 PRs in complex with ATV, NFV, and SQV. These HIV-1 PRs were labeled as PR(#1), PR(#2), and PR(#3). Further, we labeled each complexes as PR(#1)-ATV, PR(#1)-NFV, PR(#1)-SQV, PR(#2)-ATV, PR(#2)-NFV, PR(#2)-SQV, PR(#3)-ATV, PR(#3)-NFV, and PR(#3)-SQV. Simulations of subtype B HIV-1 PR in complex with ATV, NFV, and SQV were also performed. This HIV-1 PR was labeled as PR(WT), and the complexes were as PR(WT)-ATV, PR(WT)-NFV, and PR(WT)-SQV. The sequence for HXB2[33] was applied to PR(WT). Simulation of PR(WT) containing the V82I mutation in complex with ATV was further performed. This HIV-1 PR was labeled as PR(V82I) and the complex of PR(V82I) and ATV was as PR(V82I)-ATV. Each initial structure for HIV-1

PR in complex with ATV, NFV and SQV was constructed from the atom coordinates of an X-ray crystal structure (Protein Data Bank (PDB) code, 2AQU, 1OHR, 1HXB)[21,34,35] and the respective mutations were introduced using the LEaP module of AMBER8. First, we downloaded the file of HIV-1 PR containing each inhibitor from PDB site. Second, the PDB file was edited to change the residue names of the mutated residues and to delete the description on the side-chain atoms of the mutated residues. Third, the coordinates of the side-chain atoms of the mutated residues were automatically generated by LEaP module. Fourth, each model was placed in a rectangular box filled with about 8000 TIP3P water molecules[36] with all of the crystal water molecules remaining. The cutoff distance for the long-range electrostatic and van der Waals energy terms was set to 12.0 Å. The expansion and shrinkage of all covalent bonds connecting to hydrogen atom were constrained using the SHAKE algorithm.[37] Periodic boundary conditions were applied to avoid the edge effect in all calculations.

Energy minimization was achieved in three steps. Initially, movement was allowed only for water molecules and ions. Next, inhibitor and mutated residues were allowed to move in addition to the water molecules and ions. In this step, the favorable configurations of the side chains of the mutated residues were obtained because steric collisions of them were minimized. Finally, all atoms were allowed to move freely. In each step, energy minimization was executed by the steepest descent method for the first 10 000 cycles and the conjugated gradient method for the subsequent 10 000 cycles. After a 0.1 ns heating calculation until 310 K using the NVT ensemble condition, a 3.0 ns equilibrating calculation was executed at 1.0 atm and at 310 K under the NPT ensemble condition with an integration time step of 2.0 fs. The calculation steps described above were performed both for two protonation states of catalytic residues, protonated D25/unprotonated D25′ and unprotonated D25/protonated D25′. Since the MD simulations showed no large fluctuations after about 2.5 ns equilibrating calculations for most of the complexes (Supporting Information Figures S2, S3), we evaluated the energies of the respective protonation states for each complex and selected the favorable one for the subsequent extended simulation. Additional 4.0 ns simulations were performed for the selected protonation state for each complex model. After 5.0 ns of the totally 7.0 ns equilibrating calculation, the MD simulations of all complexes showed little fluctuations (Supporting Information Figures S3, S4).

As for the complexes of PR(V82I)-ATV, the protonation state was determined in the same manner, using the simulation data for 3.0 ns. The 7.0 ns MD simulation was performed for the protonation state of unprotonated D25/protonated D25′. Additionally other 7.0 ns MD simulations were executed for protease only models, that is, PR(#1), PR(#2), and PR(#3) without inhibitors for the sake of comparison in structure.

Protonation State of Catalytic Residues. Protonation states of the catalytic aspartic acids D25 and D25′ of HIV-1 PR vary depending on the binding of inhibitor or the type of HIV-1 PR.[38] Thus, appropriate protonation states of the catalytic aspartic acids should be determined for each model. We considered two kinds of protonation states.[39−41] One is a combination of protonated D25/unprotonated D25′ states, and the other is the opposite combination. To determine the protonation states when each inhibitor is bound to each HIV-1 PR, the free energies of two kinds of protonation states were compared using calculation data obtained for the last 0.5 ns of 3.0 ns MD simulations. The free energies were calculated by the MM/PBSA method,[42,43] only for the inhibitor-PR complex without subtracting the values for inhibitor only and/or unbound PR. The same parameter set as used in the equilibrating calculations was adopted for computing electrostatic and van der Waals energy terms, and no cutoff was applied for the calculation. Since the dielectric constants for the interior of proteins is considered to be in the range of 2 to 4, the interior dielectric constant was set to 2.0.[41] The outside dielectric constant was set to 80.0. The pbsa module of AMBER8 was used to solve the Poisson-Boltzmman (PB) equation. PR(WT)-ATV, PR(WT)-SQV, PR(#1)-ATV, PR(#1)-NFV, PR(#1)-SQV, PR(#2)-ATV, PR(#2)-NFV, PR(#2)-SQV, PR(#3)-ATV, and PR(#3)-SQV have been found to favor the combination of protonated D25 and unprotonated D25′. The other complexes, PR(WT)-NFV and PR(#3)-NFV, prefer the combination of unprotonated D25 and protonated D25′ (Supporting Information Table S2).

Binding Free-Energy Calculation. The binding free energy[44] was calculated by the following equation

$$\Delta G_b = \Delta E_{int}^{ele} + \Delta E_{int}^{vdw} + \Delta G_{sol} - T\Delta S_v$$

where ΔG_b is the binding free energy in solution, ΔE_{int}^{ele} and ΔE_{int}^{vdw} are electrostatic and van der Waals interaction energies between an inhibitor and a protein, ΔG_{sol} is the solvation energy, and $T\Delta S_v$ is the contribution of vibrational entropy. The parameters for cutoff and dielectric constant were the same as those used in determining the protonation state. The snapshot structures were obtained every 10 ps from the trajectories of the last 1.0 ns simulation to calculate the terms ΔE_{int}^{ele}, ΔE_{int}^{vdw}, and ΔG_{sol}. The vibrational entropic term $T\Delta S_v$ was calculated using nmode module of AMBER9 at 310 K. The snapshot structures were collected every 50 ps from the last 1.0 ns trajectories to estimate $T\Delta S_v$. The modified GB model developed by Onufriev, Bashford, and Case[45] was used to calculate the solvation energy term. The MM/GBSA results were highly correlated with the MM/PBSA results, as we described previously.[30] To examine the energetic contribution of each residue, the energy without vibrational entropy was decomposed into the contribution from each individual residue by the MM/GBSA method.

Hydrogen Bond Criteria. The formation of a hydrogen bond was defined in terms of distance and orientation. The combination of donor D, hydrogen H, and acceptor A atoms with a D−H···A configuration was regarded as a hydrogen bond when the distance between donor D and acceptor A was shorter than 3.5 Å and the angle H−D−A was smaller than 60.0°.

Results

Sequence of HIV-1 PRs. We investigated three clinically isolated HIV-1s. Two of them, #1 and #2, were isolated from patients who had no experience in the treatment with any PR inhibitors. The other, #3, was isolated from a patient who failed in treatment with NFV. In this study, we labeled PRs of these clinically isolated HIV-1s as PR(#1), PR(#2), and PR(#3). The PR of subtype B HXB2 strain[33] was labeled as PR(WT).

The amino acid sequence of each PR was compared with that of PR(WT). PR(#1) has 14 amino acid mutations, T12S, K14R, I15V, L19I, K20R, M36I, N37D, R40K, R57K, L63P, H69K, V82I, L89M, and I93L, and PR(#2) has 13 amino acid mutations, T12P, I15V, K20R, M36I, N37K, R40N, R57K, Q61E, L63T, H69K, T74S, L89M, and I93L (Figure 1B). All these mutated residues are located at the nonactive site of PR, except for V82I of PR(#1). According to HIVdb of Stanford University,[23] both kinds of PRs have no primary mutations that

TABLE 1: Prediction of Susceptibility of the Inhibitors against the Clinically Isolated PRs[a]

	ATV	NFV	SQV
PR(#1)	susceptible	susceptible	susceptible
PR(#2)	slightly resistant	susceptible	susceptible
PR(#3)	slightly resistant	resistant	susceptible

[a] An inhibitor is judged to be susceptible, slightly resistant, or resistant when the binding free energy to a PR is lower than 2 kcal/mol, higher by 2−5 kcal/mol, or higher more than 5 kcal/mol compared with that of the wild-type PR, respectively.

are highly involved in the resistance against PR inhibitors. In contrast, PR(#3) has D30N, M46L, and N88D mutations that are primary mutations for drug resistance and also one secondary mutation L10F (Figure 1B). PR(#3) further contains nine amino acid mutations, T12S, I13V, I15V, L19I, E35D, M36V, R40K, H69K, and L89I. It has also already been reported that some mutations such as K20R, M36I/V, and H69K are related to resistance against PR inhibitors and these mutations are seen in polymorphisms.[22,23]

Computational Prediction of the Susceptibility of Inhibitors. The susceptibility of three kinds of inhibitors for the respective isolated HIV-1 PRs are judged from our simulation and summarized in Table 1. This judgment is based on the difference in binding free energy between the complexes with the isolated and wild-type PRs, which is presented as $\Delta\Delta G_b$ in Table2. In PR(#1), no energetic disadvantage is observed for NFV and SQV, and the energetic disadvantage is negligible for ATV compared to PR(WT). Therefore, all PR inhibitors are concluded to be susceptible to this variant. In PR(#2), an energetic disadvantage is observed only for the complex with ATV. Hence this mutant is judged to be weakly resistant only to ATV. PR(#3) shows the energetic disadvantage for ATV and NFV and is concluded to be resistant to these two inhibitors.

To support the judgment on the above prediction for susceptibility, the statistical analysis was carried out on the data for the binding energy calculation.[46] All the computed sampling data for the binding free energy were confirmed to be in the normal distribution. The f test with a significance level of 0.05 was performed to examine whether the data have the different variance or not between WT and each mutant for the respective inhibitors. Since the hypothesis was rejected for ATV and SQV for all the mutants, the computed sampling data for ATV and SQV were concluded to have the same variance between WT and each mutant. Therefore, Student's t test was applied for ATV and SQV, while Welch's t test was for NFV. According to the Student's t test with a significance level of 0.01, the means of the binding free energies for PR(#2)-ATV and PR(#3)-ATV were different from that for PR(WT)-ATV. For PR(#1)-ATV, the null hypothesis was not rejected even with a significance level of 0.05. The Welch's t test with a significance level of 0.01 indicated that the means of the binding free energies for PR(#1)-NFV and PR(#3)-NFV were different from that of PR(WT)-NFV. The Student's t test with a significance level of 0.01 suggested the difference of the means of the binding free energies for PR(#1)-SQV and PR(#2)-SQV compared to that for PR(WT)-SQV.

Binding Free Energy. Table 2 shows the detailed energy values in the computation of the binding free energy for the complexes of the respective PRs and three kinds of inhibitors. PR(#1) contains no primary mutations known for resistance to subtype B virus. The energy gain in $\Delta\Delta G_b$ is observed for NFV and SQV compared to PR(WT), and the calculation shows a slight energy loss for ATV. PR(#2) also contains no primary mutations and the energy gain in $\Delta\Delta G_b$ is seen only for NFV and SQV. Namely PR(#1) and PR(#2) show similar change in binding energy. Since PR(#3) was isolated from the patient who failed in the NFV treatment, it is straightforwardly understood that a large energy loss in $\Delta\Delta G_b$ is observed for the complex with NFV. PR(#3) also shows the energy loss for ATV, compared to that for PR(WT). For the purpose of examining the effect of single mutation, another MD simulation was performed for the PR in which an amino mutation of V82I was introduced in PR(WT). The complex of PR(V82I) and ATV showed no disadvantage in binding free energy compared to PR(WT).

Table 2 indicates that the electrostatic term mainly dominates the binding affinity of the complex while the vibrational entropic term has some degree of influence. As for the complexes showing the increase in binding affinity, the entropic term considerably contributes to the stability of the complex in PR(#1)-SQV and PR(#2)-SQV while van der Waals interaction enhances the stability of the complexes of PR(#1)-ATV and PR(#2)-NFV. The balance of the contributions of electrostatic, van der Waals, and entropic terms also varies for the complexes showing the decrease in binding affinity. PR(#2)-ATV exhibits energetic disadvantage in van der Waals term while PR(#3)-NFV and PR(#3)-SQV show the disadvantage in the electrostatic term. The standard deviation in binding free energy calculation is considerably large. Particularly the standard deviation of entropic term is large compared to $\Delta\Delta G_b$. Accordingly, we must be careful for the interpretation of the calculated binding free energy.

Hydrogen Bonding Networks. All direct and one-water-molecule-mediated hydrogen bonds between HIV-1 PR and inhibitor were examined for every complex (Supporting Information Tables S3−S6). To survey the formation of hydrogen bonds, we sampled 1000 snapshot structures from the trajectory of the last 1.0 ns MD simulation. In all cases, the hydroxyl group existing at the center of the inhibitors makes a direct hydrogen bond to D25 or D25′ of PR. I50 or I50′ residue of PRs keeps an one-water-molecule-mediated hydrogen bond to the inhibitor. Furthermore, different hydrogen bond networks are observed among PR(#1), PR(#2), PR(#3), and PR(WT) in complex with each inhibitor.

Direct hydrogen bonds from ATV are connected to D29′ and G48′ in PR(WT)-ATV. PR(#1) hardly has the direct hydrogen bond to ATV. PR(#2) keeps the hydrogen bond to G48′ and D29′, while the hydrogen bond to D29′ is weakened. PR(#3) loses both hydrogen bonds seen in PR(WT), whereas a new hydrogen bond to D29 appears. As for NFV, PR(WT) has a direct hydrogen bond between the side chain of D30 and NFV. This hydrogen bond is kept in PR(#1)-NFV and PR(#2)-NFV. Although D30 was substituted for N30 in PR(#3), the side chain of N30 still keeps hydrogen bond to NFV. As for SQV, G48 in PR(WT) forms a direct hydrogen bond to SQV. In PR(#1)-SQV, G48 and D30 make direct hydrogen bonds to SQV. G48 in PR(#2) keeps a hydrogen bond to SQV as well as PR(WT). In contrast, the hydrogen bond from N2 of SQV disappears in PR(#3).

Change in Conformation of PRs and Inhibitors. The averaged structures of PR and inhibitor in each model were compared with those for the complex in PR(WT). The averaged structure was obtained from 1000 snapshot structures during the last 1.0 ns MD simulation. To compare the structure with that of PR(WT), the averaged structure of each mutant was superimposed on PR(WT) in respect of atom coordinates of N, Cα, and C atoms and, then, the root-mean-square deviation

TABLE 2: Binding Free Energy of the Complex of HIV-1 PR and Its Inhibitor

	ΔG_{int}^{ele}(kcal/mol)	ΔG_{int}^{vdw}(kcal/mol)	ΔG_{sol} (kcal/mol)	$-T\Delta S$ (kcal/mol)	ΔG_b (kcal/mol)	$\Delta\Delta G_b$ (kcal/mol)[a]
PR(WT)-ATV	−15.7 ± 1.7	−74.1 ± 3.5	11.6 ± 1.5	26.2 ± 7.5	−52.0	
PR(WT)-NFV	−24.2 ± 2.1	−66.9 ± 4.2	12.5 ± 1.7	29.1 ± 6.8	−49.5	
PR(WT)-SQV	−15.1 ± 2.9	−70.1 ± 4.3	10.0 ± 1.3	31.1 ± 6.0	−44.1	
PR(#1)-ATV	−12.8 ± 2.2	−79.9 ± 3.0	12.9 ± 1.1	28.8 ± 8.6	−51.0	+1.0
PR(#1)-NFV	−18.4 ± 3.0	−72.2 ± 3.4	11.9 ± 1.5	25.0 ± 9.0	−53.7	−4.2
PR(#1)-SQV	−21.7 ± 4.2	−72.4 ± 3.9	13.6 ± 1.7	27.0 ± 9.6	−53.5	−9.4
PR(#2)-ATV	−17.7 ± 3.6	−70.5 ± 4.1	12.8 ± 1.9	27.0 ± 5.8	−48.4	+3.6
PR(#2)-NFV	−20.0 ± 5.9	−69.1 ± 2.8	13.0 ± 1.2	26.2 ± 7.4	−49.9	−0.4
PR(#2)-SQV	−16.6 ± 3.5	−67.9 ± 4.7	10.6 ± 1.8	25.6 ± 8.6	−48.3	−4.2
PR(#3)-ATV	−12.2 ± 2.1	−76.5 ± 3.6	12.0 ± 1.2	28.2 ± 7.4	−48.5	+3.5
PR(#3)-NFV	−13.1 ± 1.9	−65.5 ± 3.2	10.5 ± 1.2	25.3 ± 6.6	−42.8	+6.7
PR(#3)-SQV	−13.0 ± 2.5	−71.5 ± 3.9	9.0 ± 0.9	30.6 ± 6.2	−44.9	−0.8
PR(V82I)-ATV	−24.4 ± 2.4	−80.8 ± 4.7	15.4 ± 1.5	23.6 ± 6.9	−66.2	−13.2

[a] Difference from PR(WT).

TABLE 3: Genotype Assay of Clinically Isolated PRs in Complex with Each Inhibitor

	ATV	NFV	SQV
PR(#1)	susceptible[a]	susceptible	susceptible
PR(#2)	susceptible	susceptible	susceptible
PR(#3)	intermediate resistance[b]	high-level resistance[c]	low-level resistance[d]

[a] Virus of this category hardly shows the reduction in susceptibility to the drug. [b] Virus of this category shows certain degree of drug resistance between the low-level and the high-level resistances. [c] Virus of this category shows the highest levels of the in vitro drug resistance and/or the patients infected with viruses of this category generally have little or no virologic response to treatment with the drug. [d] Virus of this category reduces the in vitro susceptibility to the drug and/or the patients with viruses of this category may have a suboptimal virologic response to treatment.

(rmsd) value was calculated (Figure 2A). Since the residues located at the outer part of PR largely fluctuate (Supporting Information Figure S6), we focused only on the structural change of the residues located near the active site of HIV-1 PRs. A prominent structural change is seen in the complexes of PR(#1)-ATV, PR(#1)-NFV, PR(#2)-NFV, and PR(#3)-NFV at the 80s loop which corresponds to 80−84th residues of PR. PR(#1)-ATV and PR(#3)-ATV show a structural change at the flap region. No significant changes are observed for the other complexes around the binding pocket. In contrast, the change in binding pose is more clearly observed for the inhibitors. In the complexes of PR(#1), the ring parts of the respective inhibitors, 3′-phenylpyridine group in ATV and phenylsulfanyl group in NFV, show large deviations, compared with that of PR(WT). These large structural deviations are also seen in the complexes of PR(#2). PR(#3) shows the deviation not only at the ring part but also for the whole part of all the inhibitors. The quinoline group in SQV shows a considerable deviation in PR(#3), while PR(#1) and PR(#2) has little change compared with PR(WT).

Discussion

PR(#1) and PR(#2). Both PR(#1) and PR(#2) were derived from the patients who were naive for the treatment with PR inhibitors. The polymorphisms at the 20th, 36th, 69th, and 93rd residues are commonly seen in both sequences of PR(#1) and PR(#2). All these amino acid mutations were reported to be involved in drug resistance of subtype B HIV-1 PR.[14−22] It is important to note that these mutations are not the primary mutation for drug resistance but the secondary mutation accompanying with some primary mutations. Hence, judging from the knowledge accumulated on subtype B PR, these mutations would not cause the drug resistance by themselves. Indeed, according to HIVdb, the genotype assay web service of Stanford University,[23] both of PR(#1) and PR(#2) were judged not to cause the resistance against the approved PR inhibitors (Table 3). Genotype assay is the prediction method for drug resistance based only on the sequence of the virus and sometimes used in the clinical scene. The calculated binding free energy of the present MD simulation has suggested an almost similar conclusion that NFV and SQV are almost effective for PR(#1) and PR(#2) as well as PR(WT). Only the assessment for PR(#2)-ATV complex is different (Table 1).

V82I Mutation. Our simulation suggests that PR(#2) is weakly resistant only for ATV (Table 1). It is informative to clarify the cause for the difference in efficacy of ATV between PR(#1) and PR(#2). A comparison in the amino sequence between PR(#1) and PR(#2) shows that V82I and V63P mutations appear only in PR(#1). Since the 82nd residue is located at the inhibitor-binding site of PR and has direct interaction with the PR inhibitors, V82I may have some degree of influence on the binding affinity between PR and its inhibitor. The 82nd residue is, further, known as a key residue relating to the recognition of substrate.[22,47−49] Accordingly, it will be important to examine the effect of the V82I mutation on the PR-ATV complex. Several previous studies with X-ray crystal analysis suggested that the 82nd residue is located at the vicinity of ring part of ATV (3′-phenylpyridil group).[21,34,35] Our present MD simulation indicates that the V82I mutation causes structural change not only in PR but also in ATV (Figure 2), which leads the stable binding pose of ATV different from that in PR(WT). In PR(WT), the side chain of V82 is positioned with facing to the inner side of the binding pocket (Figure 3A). In contrast, the side chain of I82 faces opposite to the binding pocket (Figure 3B). Furthermore, 3′-phenylpyridyl group of ATV occupies the different space compared to PR(WT). 3′-phenylpyridyl group interacts with the flap region around the 50th residues in PR(WT), while this group is shifted toward I84 in PR(#1). This shift will increase the van der Waals interaction between PR and ATV (Table 2) and, further, induces the formation of hydrogen bond between D25 and ATV (Supporting Information, Tables S3 and S4). The binding free energy for the ATV-PR complex was decomposed into the contributions from the respective residues (Supporting Information, Figure S8). A comparison of the decomposed binding energies of PR(#1), PR(#2), PR(#3) with PR(WT) indicated that noticeable energy loss appears around the residues of A28′, D29′, G48′, and T80′. Inversely, energy gain is observed at the residue of R8 and D29. All these amino residues are located at the active site, and the

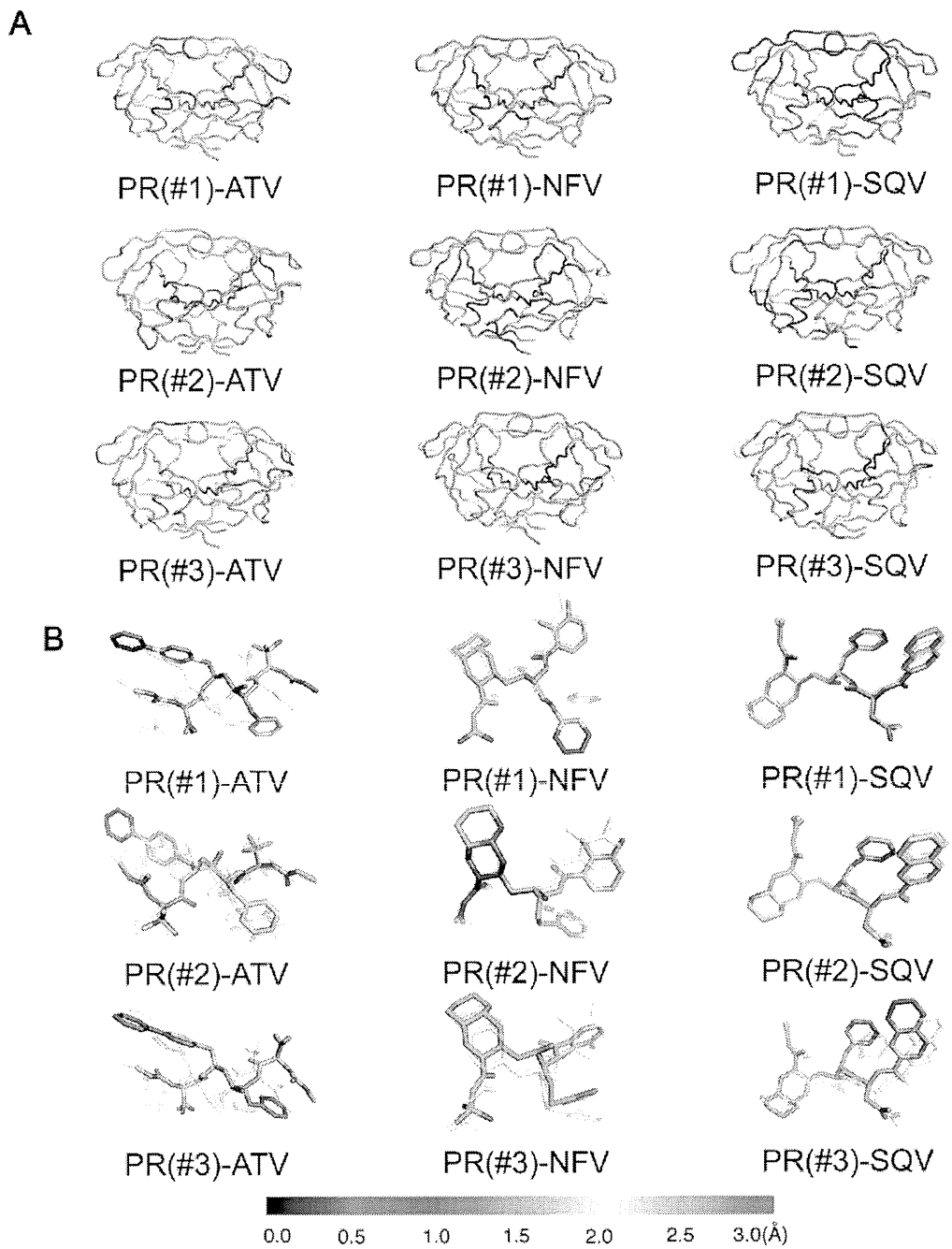

Figure 2. (A) Three-dimensional plot of rmsd of the average structure of each PR measured from PR(WT). PRs are shown in the colored tube representation. (B) Three-dimensional plot of rmsd of the average structure of each PR inhibitor measured from PR(WT). Inhibitors are shown in the colored stick representation. The color means the magnitude of rmsd shown in the bottom bar. The superimposed gray tubes in A and sticks in B represent the structure in PR(WT).

energy changes were mainly caused by the displacement of the binding position of ATV.

In order to examine whether the above structural changes are indeed caused by the V82I mutation, we executed another 3.0 ns MD simulation on PR(V82I)-ATV complex, where PR(V82I) model was constructed by introducing the V82I mutation into PR(WT). This simulation on PR(V82I) shows that the side chain of V82I faces opposite to the binding pocket and 3′-phenylpyridyl group of ATV is shifted toward I84 (Figure 3C). Our energy calculation shows no loss in binding free energy both in PR(#1) and PR(V82I) (Table 2). That is, the V82I mutation causes the structural change, but no decrease in binding affinity. In contrast to PR(#1), PR(#2) does not contain the V82I mutation and PR(#2)-ATV complex shows the loss in binding free energy compared to PR(WT). In the binding structure of the PR(#2)-ATV complex, 3′-phenylpyridyl group of ATV is slightly shifted as well as PR(#1), but the 82nd residue is not completely shifted from the original position (Figure 3D). Because of the slight positional shift, 3′-phenylpyridyl group still keep the interaction with the flap region of PR in a similar manner with PR(WT). This halfway position of ATV is energetically unfavorable. Therefore, we can conclude that the V82I mutation causes the alteration of the position of side chain of I82 and the shift of ring part of ATV toward 80′ loop. This

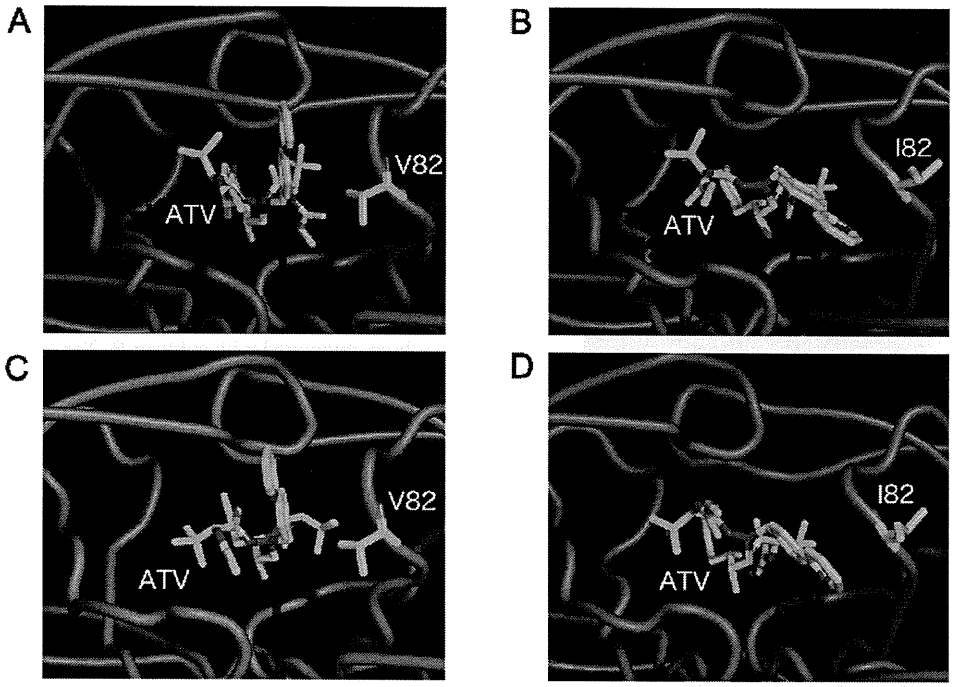

Figure 3. Structure of ATV and the 82nd residue in each model. ATV and the residue are shown by sticks and PR is by tubes. (A) PR(WT)-ATV, (B) PR(#1)-ATV, (C) PR(#2)-ATV, (D) PR(V82I)-ATV.

shift keeps the energetic stability of the complex of PR and ATV. The presence of the V82I mutation exerts a strong influence on the binding with ATV and one of the prominent characteristics for subtype C HIV-1 PR.

PR(#3). Since PR(#3) was derived from the patient who failed in the treatment with NFV, PR(#3) contains mutations known to confer resistance against NFV. The genotype assay based on the HIVdb of Stanford University suggested the resistance to NFV and, further, indicated the resistance to ATV and SQV. The calculated binding free energy in our present work gave a similar conclusion. That is, a large loss in binding free energy is observed for the PR(#3)-NFV complex, compared with PR(WT), and the energy loss is also seen for the complexes with ATV. The D30N mutation appearing in PR(#3) is well-known as the primary mutation causing the resistance against NFV and frequently seen in the patient who was infected with subtype B HIV-1 and failed in the treatment with NFV.[22,50] In subtype B HIV-1 PR, the break of the hydrogen bond between the side chain of N30 and NFV due to the D30N mutation is the main reason for causing resistance to NFV.[30,51,52] The hydrogen bond between the side chain of N30 and NFV is, however, maintained in PR(#3) in contrast with the subtype B D30N-mutated PR (Supporting Information, Tables S3 and S6). As our previous simulation on the D30N/M36 V doubly mutated subtype B PR suggested, the M36 V mutation in PR(#3), which is also reported to be involved in resistance to NFV,[13] will induce the formation of hydrogen bonds between NFV and N30.[52] Therefore, the M36 V mutation is effective for keeping the hydrogen bond both in subtype B and subtype C PRs. The hydrogen bond was observed to disappear for a while for 7.0 MD simulation and the m-phenyl group of NFV was occasionally change its position in the PR(#3)-NFV complex. This means that the chain of N30 cannot make a strong hydrogen bond with m-phenyl group of NFV compared to D30. This will be a reason for low binding affinity of NFV to PR(#3).

In the PR(#3)-ATV complex, the binding free energy was diminished compared to PR(WT) due to the shift of the binding position of ATV. This position shift is reflected in the disappearance of hydrogen bonds seen in PR(WT) and the appearance of another direct hydrogen bond between D29 and O2 of ATV (Supporting Information, Table S6). No energy loss was observed in the PR(#3)-SQV complex. This result is compatible with the findings that PR(#3) contains few mutations related to SQV resistance.[22]

D30N Mutation. PR(#3) is the subtype C HIV-1 PR containing the D30N mutation. The appearance of the D30N mutation was, however, reported to be rare in the subtype C HIV-1 showing the drug resistance to NFV.[13,18,25,26] Therefore, it is informative to clarify the reason why the D30N mutation rarely appears in subtype C HIV-1 PR from the structural viewpoint. Some experimental findings indicated that the rare appearance of the D30N mutation in subtype C HIV-1 PR is closely related to the replication ability of the virus.[25,26] The replication ability of subtype C HIV-1 containing the D30N/N88D mutation was lower than the variant containing the L90 M mutation, though the D30N/N88D and L90 M mutations are known as the primary mutation conferring resistance against NFV in subtype B HIV-1.[26] It has been reported that the 29th and 87th residues in PR are related to the stability of dimer formation.[53,54] Considering this finding, we paid our attention to the structure of the 29th and 87th residues in the PR(#3)-NFV complex. If the structural stability of HIV-1 PR is reduced, the enzymatic activity of PR to cleave the peptide linkage of substrate will be seriously lowered. The low enzymatic activity will lead to the decrease in replication ability. It was found that the side chain of D29 was shifted toward the inner side of the binding pocket in PR(#3)-NFV, compared to PR(WT)-NFV (Figure 4A,B). Further, the side chain of R87 was displaced opposite to the binding pocket. Our previous simulations suggested that the mutation at the 36th residue influences the geometry of D29.[51] Hence, in order to further examine the influence of the M36 V mutation on the 29th and 87th residues, we have performed another MD simulation on the complex of NFV and PR(WT) containing the D30N/M36 V mutation. This

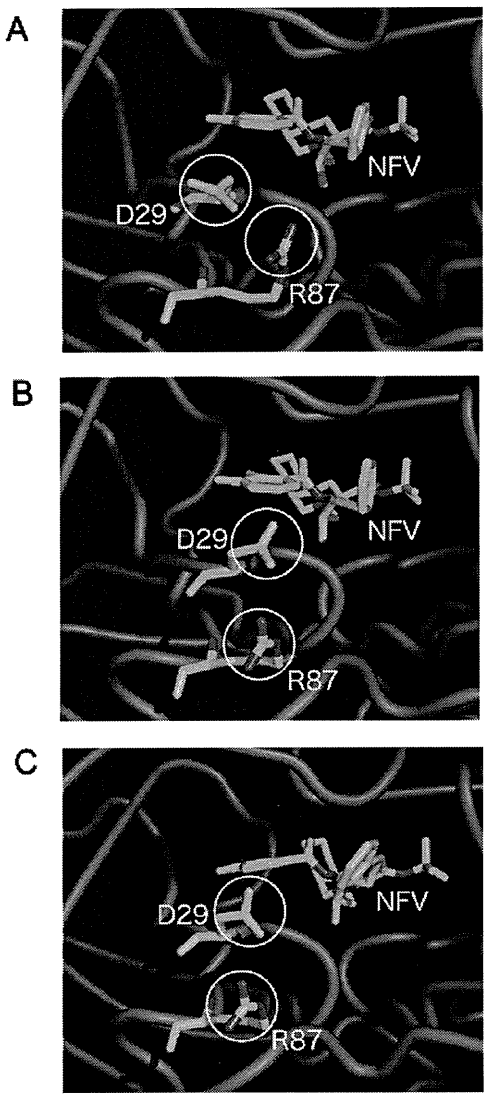

Figure 4. Structure of NFV and the 29th and 87th residues. ATV and the residues are shown by sticks and PR is by tubes. (A) PR(WT)-NFV, (B) PR(#3)-NFV, (C) PR(D30N/M36 V)-NFV.

simulation showed a structural change at the side chains of the 29th and 87th residues as well as PR(#3) (Figure 4C). Accordingly, we conclude that the D30N/M36 V mutation causes the position shift of the side chains of the 29th and 87th residues in the subtype C HIV-1 PR, which induces the structural instability of HIV-1 PR and leads to the lowering of the enzymatic activity of PR. This low enzymatic activity results in the decrease of the replication ability of HIV-1. Since the replication rate of subtype C virus containing the D30N mutation is low, most of the subtype C HIV-1s resistant to NFV rarely contain the D30N mutation.

Overall Picture of the Structure of Subtype C HIV-1 Protease. On the basis of the results of the present MD simulation, we have proposed the influence of polymorphisms of subtype C HIV-1 PR on the susceptibility of drugs. The discussion was mainly developed from the viewpoint of complex structure of PR and inhibitor. A comparison of structures of PRs with and without the inhibitors clearly shows the difference at the flap region (Supporting Information, Figure S7). The flap tips were displaced upward due to the association with the inhibitor in every complex. This displacement is particularly evident in PR(#1) and PR(#2). PR(#3) markedly shows the displacement at the flap elbow and fulcrum loop (Supporting Information, Figure S6).

The X-ray crystal analysis is one of the most powerful techniques to investigate the structure of protein. Recently a crystallization of the subtype C PR was achieved by Coman et al.[54,55] Their first report provided the information on the X-ray crystal structure of the subtype C PR complexed with two kinds of inhibitors, indinavir (IDV) and NFV.[55] Their second report gave a comparison between the inhibitor-unbound subtype C and B PRs.[56] The unbound subtype C PR exhibited a larger distance between the two flap tips, a downward displacement of the 36−41's loop, and an increased thermal stability of the 10s loop, compared with subtype B. The increase of the distance of the flap tips is seen in the PR(#1)-ATV and PR(#3)-NFV complexes in our present simulation and the downward displacement of the 36−41's loop is obvious in the PR(#1)-ATV, PR(#2)-NFV, PR(#3)-ATV and PR(#3)-SQV complexes (Figure 2). The increase of stability of the 10s loop is observed in PR(#1)-SQV, PR(#3)-NFV, and PR(#3)-SQV (Supporting Information, Figure S6). Therefore, some of the structural characteristics are compatible with between the X-ray crystal structure and our simulation results. Our calculation will also suggest the drug efficacy of the respective inhibitors on the clinically isolated subtype C PRs. Since structural findings give an insight into the drug resistance, viral fitness, and the response to therapy, it will be required to accumulate much information about the complex structures of the nonsubtype B HIV-1 PRs and inhibitors both from experimental and theoretical approaches. The accumulated data will be useful for the proper choice of inhibitors, which enhances the performance of anti-HIV therapy for the patients infected with the nonsubtype B virus.

Conclusion

MD simulations on the complexes of subtype C HIV-1 PR and three kinds of approved inhibitors were carried out to investigate the influence of natural polymorphisms of subtype C on the change in binding affinity with the inhibitors. The simulation suggested that ATV occasionally decreases the susceptibility to the subtype C HIV-1 PRs. The presence of the V82I polymorphism affects the structural stability of the complex, which is related to the decrease of the susceptibility of ATV. The subtype C HIV-1 PR containing the D30N mutation will confer drug resistance even for the variant containing the M36 V mutation. This is a difference from the subtype B HIV-1 PR. Our MD simulation provided the reason why the emergence rate of the D30N mutation is low for subtype C HIV-1 PR. The low emergence rate is interpreted as a result from the decrease of HIV-1 replication ability of the D30N containing variant.

Acknowledgment. This work was supported by Grant-in-Aid for Scientific Research (C) from Japan Society for the Promotion of Science (JSPS) and by a Health and Labor Science Research Grant for Research on Publicly Essential Drugs and Medical Devices from the Ministry of Health and Labor of Japan. One of the authors (H.O.) gratefully acknowledges the postdoctoral research fellowship from JSPS. A part of this work was also supported by a grant from the Futaba Electronics Memorial Foundation.

Supporting Information Available: Description on the amino sequence of the isolated samples, a list of hydrogen bond networks, the determination of protonation states of catalytic

aspartic acids, B-factors of the respective residues in simulation, comparison of structures with and without the inhibitors, rmsd plots during MD simulations, and the results of principal component analyses were provided. This material is available free of charge via the Internet at http://pubs.acs.org.

References and Notes

(1) Joint United Nations Programme on HIV/AIDS (UNAIDS). 2007 AIDS Epidemic Update UNAIDS. 2007.

(2) Kräusslich, H. G.; Wimmer, E. *Annu. Rev. Biochem.* **1988**, *57*, 701.

(3) Kohl, N. E.; Emini, E. A.; Schleif, W. A.; Davis, L. J.; Heimbach, J. C.; Dixon, R. A.; Scolinick, E. M.; Sigal, I. S. *Proc. Natl. Acad. Sci. U.S.A.* **1988**, *85*, 4686.

(4) Craig, J. C.; Duncan, I. B.; Hockley, D.; Grief, C.; Roberts, N. A.; Mills, J. S. *Antiviral Res.* **1991**, *16*, 295.

(5) Vacca, J. P.; Dorsey, B. D.; Schleif, W. A.; Leven, R. B.; McDaniel, S. L.; Darke, P. L.; Zugay, J.; Quintero, J. C.; Blahy, O. M.; Roth, E.; Sardana, V. V.; Schlabach, A. J.; Graham, P. I.; Condra, J. H.; Gotlib, L.; Holloway, M. K.; Lin, J.; Chen, L.-W.; Vastag, K.; Ostvic, D.; Anderson, P. S.; Emini, E. A.; Huff, J. R. *Proc. Natl. Acad. Sci. U.S.A.* **1994**, *91*, G4096.

(6) Kempf, D. J.; Marsh, K. C.; Denissen, J. F.; McDonald, E.; Vasavanonda, S.; Flentga, C. A.; Green, B. E.; Fino, L.; Park, C. H.; Kong, X.; Wideburg, N. E.; Saldivar, A.; Ruiz, L.; Kati, W. M.; Sham, H. L.; Robins, T.; Stewart, K. D.; Hsu, A.; Plattner, J. J.; Leonard, J. M.; Norbeck, D. W. *Proc. Natl. Acad. Sci. U.S.A.* **1995**, *92*, 2484.

(7) Livington, D. J.; Pazhanisamy, S.; Porter, D. J.; Partaledis, J. A.; Tung, R. D.; Painter, G. R. *J. Infect. Dis.* **1995**, *172*, 1238.

(8) Patick, A. K.; Mo, H.; Markowitz, M.; Appelt, K.; Wu, B.; Musick, L.; Kalish, V.; Kaldor, S.; Reich, S.; Ho, D.; Webber, S. *Antimicrob. Agents Chemother.* **1996**, *40*, 292 Erratum, 40, 1575.

(9) Carrillo, A.; Stewart, K. D.; Sham, H. L.; Norbeck, D. W.; Kohlbrenner, W. E.; Leonard, J. M.; Kempf, D. J.; Molla, A. J. *J. Virol.* **1998**, *72*, 7532.

(10) Robinson, B. S.; Riccardi, K. A.; Gong, Y. F.; Guo, Q.; Stock, D. A.; Blair, W. S.; Terry, B. J.; Deminie, C. A.; Djang, F.; Colonno, R. J.; Lin, P. F. *Antimicrob. Agents Chemother.* **2000**, *44*, 2093.

(11) Larder, B. A.; Hertogs, K.; Bloor, S.; van den Eynde, C.; DeCian, W.; Wang, Y.; Freimuth, W. W.; Tarpley, G. *AIDS* **2000**, *14*, 1943.

(12) Koh, Y.; Nakata, H.; Maeda, K.; Ogata, H.; Bilcer, G.; Devasamudram, T.; Kincaid, J. F.; Boross, P.; Wang, Y. F.; Tie, Y.; Volarath, P.; Gaddis, L.; Harrison, R. W.; Weber, I. T.; Ghosh, A. K.; Mitsuya, H. *Antimicrob. Agents Chemother.* **2003**, *47*, 3123.

(13) Kantor, R.; Katzenstein, D. A.; Efron, B.; Carvalho, A. P.; Wynhoven, B.; Cane, P.; Clarke, J.; Sirivichayakul, S.; Soares, M. A.; Snoeck, J.; Pillay, C.; Rudich, H.; Rodrigues, R.; Holguin, A.; Ariyoshi, K.; Bouzas, M. B.; Cahn, P.; Sugiura, W.; Soriano, V.; Brigido, L. F.; Grossman, Z.; Morris, L.; Vandamme, A. M.; Tanuri, A.; Phanuphak, P.; Weber, J. N.; Pillay, D.; Harrigan, P. R.; Camacho, R.; Schapiro, J. M.; Shafer, R. W. *PLoS Med.* **2005**, *2*, 325.

(14) Cornelissen, M.; van den Burg, R.; Zorgdrager, F.; Lukashov, V.; Goudsmit, J. *J. Virol.* **1997**, *71*, 6348.

(15) Pieniazek, D.; Rayfield, M.; Hu, D. J.; Nkengasong, J.; Wiktor, S. Z.; Downing, R.; Biryahwaho, B.; Mastro, T.; Tanuri, A.; Soriano, V.; Lal, R.; Dondero, T. *AIDS* **2000**, *14*, 1489.

(16) Vergne, L.; Peeters, M.; Mpoudi-Ngole, E.; Bourgeois, A.; Liegeois, F.; Toure-Kane, C.; Mboup, S.; Mulanga-Kabeya, C.; Saman, E.; Jourdan, J.; Reynes, J.; Delaporte, E. *J. Clin. Microbiol.* **2000**, *38*, 3919.

(17) (a) Grossman, Z.; Vardinon, N.; Chemtob, D.; Alkan, M. L.; Bentwich, Z.; Burke, M.; Gottesman, G.; Istomin, V.; Levi, I.; Maayan, S.; Shahar, E.; Schapiro, J. M. *AIDS* **2001**, *15*, 1453. (b) Grossman, Z.; Vardinon, N.; Chemtob, D.; Alkan, M. L.; Bentwich, Z.; Burke, M.; Gottesman, G.; Istomin, V.; Levi, I.; Maayan, S.; Shahar, E.; Schapiro, J. M. *AIDS* **2001**, *15*, 2209.

(18) Cane, P. A.; de Ruiter, A.; Rice, P.; Wiselka, M.; Fox, R.; Pillay, D. *J. Clin. Microbiol.* **2001**, *39*, 2652.

(19) Zhong, P.; Kang, L.; Pan, Qichao.; Koings, F.; Burda, S.; Ma, L.; Xue, Y.; Zheng, X.; Jin, Z.; Nyambi, P. *JAIDS, J. Acquired Immune. Defic. Syndr.* **2003**, *34*, 91.

(20) Ariyoshi, K.; Matsuda, M.; Miura, H.; Tateishi, S.; Yamada, K.; Sugiura, W. *AIDS, J. Acquired Immune. Defic. Syndr.* **2003**, *33*, 336.

(21) Clemente, J. C.; Coman, R. M.; Thiaville, M. M.; Janka, L. K.; Jeung, J. A.; Nukoolkarn, S.; Govindasamy, L.; Agbandje-McKenna, M.; McKenna, R.; Leelamanit, W.; Goodenow, M. M.; Dunn, B. M. *Biochemistry* **2006**, *45*, 5468.

(22) Johnson, V. A.; Brun-Vézinet, F.; Clotet, N.; Günthard, H. F.; Kuritzkes, D. R.; Pillay, D.; Schapiro, J. M.; Richman, D. D. *Top. HIV Med.* **2008**, *16*, 62.

(23) Rhee, S.-Y.; Gonzales, M. J.; Kantor, R.; Betts, B. J.; Ravela, J.; Shafer, R. W. *Nucleic Acids Res.* **2003**, *31*, 298.

(24) Velazquez-Campoy, A.; Todd, M. T.; Vega, S.; Freire, E. *Proc. Natl. Acad. Sci. U.S.A.* **2001**, *98*, 6062.

(25) Grossman, Z.; Paxinos, E. E.; Averbuch, D.; Maayan, S.; Parkin, N. T.; Dan, E.; Margalit, L.; Valery, I.; Shaked, Y.; Mendelson, E.; Ram, D.; Petropoulos, C. J.; Schapiro, J. M. *Antimicrob. Agents Chemother.* **2004**, *48*, 2159.

(26) Gonzalez, L. M. F.; Brindeiro, R. M.; Aguiar, R. S.; Pereira, H. S.; Abreu, C. M.; Soares, M. A.; Tanuri, A. *Antimicrob. Agents Chemother.* **2004**, *48*, 3552.

(27) Case, D. A.; Darden, T. A.; Cheatham, T. E., III; Simmerling, C. L.; Wang, J.; Duke, R. E.; Luo, R.; Merz, K. M.; Wang, B.; Pearlman, D. A.; Crowly, M.; Brozell, S.; Tsui, V.; Gohlke, H.; Mongan, J.; Hornak, V.; Cui, G.; Beroza, P.; Schafmeister, C.; Caldwell, J. W.; Ross, W. S.; Kollman, P. A. *Amber 8*; University of California: San Francisco, CA, 2004.

(28) Duan, Y.; Wu, C.; Chowdhury, S.; Lee, M. C.; Xiong, G.; Zhang, W.; Yang, R.; Cieplak, P.; Luo, R.; Lee, T. *J. Comput. Chem.* **2003**, *24*, 1999.

(29) (a) Wang, J.; Wolf, R. M.; Caldwell, J. W.; Kollman, P. A.; Case, D. A. *J. Comput. Chem.* **2004**, *25*, 1157. (b) Wang, J.; Wolf, R. M.; Caldwell, J. W.; Kollman, P. A.; Case, D. A. *J. Comput. Chem.* **2005**, *26*, 114.

(30) Ode, H.; Matsuyama, S.; Hata, M.; Hoshino, T.; Kakizawa, J.; Sugiura, W. *J. Med. Chem.* **2007**, *50*, 1768.

(31) Cieplak, P.; Cornell, W. D.; Bayly, C.; Kollman, P. A. *J. Comput. Chem.* **1995**, *16*, 1357.

(32) Frisch, M. J. Trucks, G. W.; Schlegel, H. B.; Scuseria, G. E.; Robb, M. A.; Cheeseman, J. R.; Montgomery, J. A., Jr.; Vreven, T.; Kudin, K. N.; Burant, J. C.; Millam, J. M.; Iyengar, S. S.; Tomasi, J.; Barone, V.; Mennucci, B.; Cossi, M.; Scalmani, G.; Rega, N.; Petersson, G. A.; Nakatsuji, H.; Hada, M.; Ehara, M.; Toyota, K.; Fukuda, R.; Hasegawa, J.; Ishida, M.; Nakajima, T.; Honda, Y.; Kitao, O.; Nakai, H.; Klene, M.; Li, X.; Knox, J. E.; Hratchian, H. P.; Cross, J. B.; Bakken, V.; Adamo, C.; Jaramillo, J.; Gomperts, R.; Stratmann, R. E.; Yazyev, O.; Austin, A. J.; Cammi, R.; Pomelli, C.; Ochterski, J. W.; Ayala, P. Y.; Morokuma, K.; Voth, G. A.; Salvador, P.; Dannenberg, J. J.; Zakrzewski, V. G.; Dapprich, S.; Daniels, A. D.; Strain, M. C.; Farkas, O.; Malick, D. K.; Rabuck, A. D.; Raghavachari, K.; Foresman, J. B.; Ortiz, J. V.; Cui, Q.; Baboul, A. G.; Clifford, S.; Cioslowski, J.; Stefanov, B. B.; Liu, G.; Liashenko, A.; Piskorz, P.; Komaromi, I.; Martin, R. L.; Fox, D. J.; Keith, T.; AlLaham, M. A.; Peng, C. Y.; Nananyakkara, A.; Challacombe, M.; Gill, P. M. W.; Johnson, B.; Chen, W.; Wong, M. W.; Gonzalez, C.; Pople, J. A. *Gaussian 03*; Gaussian, Inc.: Wallingford, CT, 2004.

(33) Ratner, L.; Haseltine, W.; Patarca, R.; Livak, K. J.; Starcich, B.; Josephs, S. F.; Doran, E. R.; Rafalski, J. A.; Whitehorn, E. A.; Baumeister, K.; Ivanoff, L.; Petteway, S. R., Jr.; Pearson, M. L.; Lautenberger, J. A.; Papas, T. S.; Ghrayebparallel, J.; Changparallel, N. T.; Gallo, R. C.; Wong-Staal, F. *Nature* **1985**, *313*, 277.

(34) Kaldor, S. W.; Kalish, V. J.; Davies, J. F.; Shetty, B. V.; Fritz, J. E.; Appelt, K.; Burgess, J. A.; Campanale, K. M.; Chirgadze, N. Y.; Clawson, D. K.; Dressman, B. A.; Hatch, S. D.; Khalil, D. A.; Kosa, M. B.; Lubbehusen, P. P.; Muesing, M. A.; Patrick, A. K.; Reich, S. H.; Su, K. S.; Tatlock, J. H. *J. Med. Chem.* **1997**, *40*, 3979.

(35) Krohn, A.; Redshaw, S.; Ritchie, J. C.; Graves, B. J.; Hatada, M. H. *J. Med. Chem.* **1991**, *34*, 3340.

(36) Jorgensen, W. L.; Chandrasekhar, J.; Madura, J. D.; Impey, R. W.; Klein, M. L. *J. Chem. Phys.* **1983**, *79*, 926.

(37) Ryckaert, J.-P.; Ciccotti, G.; Berendsen, H. J. C. *J. Comput. Phys.* **1977**, *23*, 327.

(38) Zoete, V.; Michielin, O.; Karplus, M. *J. Mol. Biol.* **2002**, *315*, 21.

(39) Roberts, N. A.; Martin, J. A.; Kinchington, D.; Broadhurst, A. V.; Craig, J. C.; Duncan, I. B.; Galpin, S. A.; Handa, B. K.; Kay, J.; Krohn, A.; Lambert, R. W.; Merrett, J. H.; Millis, J. S.; Parkes, K. E. B.; Redshaw, S.; Ritchie, A. J.; Taylor, D. L.; Thomas, G. L.; Machin, P. J. *Science* **1990**, *248*, 358.

(40) Okimoto, N.; Tsukui, T.; Hata, M.; Hoshino, T.; Tsuda, M. *J. Am. Chem. Soc.* **1999**, *121*, 7349.

(41) Wang, W.; Kollman, P. A. *J. Mol. Biol.* **2000**, *303*, 567.

(42) Srinivasan, J.; Cheatham, T. E., III; Kollman, P.; Case, D. A. *J. Am. Chem. Soc.* **1998**, *120*, 9401.

(43) Kollman, P. A.; Massova, I.; Reyes, C.; Kuhn, B.; Huo, S.; Chong, L.; Lee, M.; Lee, T.; Duan, Y.; Wang, W.; Donini, O.; Cieplak, P.; Srinivasan, J.; Case, D. A.; Cheatham, T. E., III *Acc. Chem. Res.* **2000**, *33*, 889.

(44) Kollman, P. *Chem. Rev.* **1993**, *93*, 2395.

(45) Onufriev, A.; Bashford, D.; Case, D. A. *Proteins: Struct., Funct., Bioinf.* **2004**, *55*, 383.

(46) Hoel, P. G. In *Introduction to Mathematical Statistics*, 5th ed.; John Wiley & Sons: New York, 1984; pp 151−160.

(47) Prabu-Jeyabalan, M.; Nalivaika, E. A.; King, N. M.; Schiffer, C. A. *J. Virol.* **2003**, *77*, 1306.

(48) Prabu-Jeyabalan, M.; Nalivaika, E. A.; King, N. M.; Schiffer, C. A. *J. Virol.* **2004**, *78*, 12446.

(49) Tie, Y.; Boross, P. I.; Wang, Y. F.; Gaddis, L.; Liu, F.; Chen, X.; Tozser, J.; Harrison, R. W.; Weber, I. T. *FEBS J.* **2005**, *272*, 5265.

(50) Sugiura, W.; Matsuda, Zene.; Yokomaku, Y.; Hertogs, K.; Larder, B.; Oishi, T.; Okano, A.; Shiino, T.; Tatsumi, M.; Matsuda, M.; Abumi, H.; Takata, N.; Shirahata, S.; Yamada, K.; Yoshikura, H.; Nagai, Y. *Antimicrob. Agents Chemother.* **2002**, *46*, 708.

(51) Ode, H.; Ota, M.; Neya, S.; Hata, M.; Sugiura, W.; Hoshino, T. *J. Phys. Chem. B.* **2005**, *109*, 565.

(52) Ode, H.; Matsuyama, S.; Hata, M.; Neya, S.; Kakizawa, J.; Sugiura, W.; Hoshino, T. *J. Mol. Biol.* **2007**, *370*, 598.

(53) Ishima, R.; Ghirlando, R.; Tözsér, J.; Gronenborn, A. M.; Torchia, D. A.; Louis, J. M. *J. Biol. Chem.* **2001**, *276*, 49110.

(54) Louis, J. M.; Ishima, R.; Nesheiwat, I.; Pannell, L. K.; Lynch, S. M.; Torchia, D. A.; Gronenborn, A. M. *J. Biol. Chem.* **2003**, *278*, 6085.

(55) Coman, R. M.; Robbins, A. H.; Goodenow, M. M.; McKenna, R.; Dunn, B. M. *Acta Crystallogr.* **2007**, *F63*, 320.

(56) Coman, R. M.; Robbins, A. H.; Goodenow, M. M.; Dunn, B. M.; McKenna, R. *Acta Crystallogr.* **2008**, *D64*, 754.

JP908314F

Bioorganic & Medicinal Chemistry 19 (2011) 816–825

Contents lists available at ScienceDirect

Bioorganic & Medicinal Chemistry

journal homepage: www.elsevier.com/locate/bmc

Structural and biochemical study on the inhibitory activity of derivatives of 5-nitro-furan-2-carboxylic acid for RNase H function of HIV-1 reverse transcriptase

Hiroshi Yanagita [a], Emiko Urano [b], Kishow Matsumoto [a], Reiko Ichikawa [b], Yoshihisa Takaesu [a], Masakazu Ogata [a], Tsutomu Murakami [b], Hongui Wu [b,c], Joe Chiba [c], Jun Komano [b], Tyuji Hoshino [a,*]

[a] Graduate School of Pharmaceutical Sciences, Chiba University, 1-33 Yayoi-cho, Inage-ku, Chiba 263-8522, Japan
[b] AIDS Research Center, National Institute of Infectious Diseases, 1-23-1 Toyama, Shinjuku, Tokyo 162-8640, Japan
[c] Faculty of Industrial Science and Technology, Tokyo University of Science, Yamazaki 2641, Noda, Chiba 278-8510, Japan

ARTICLE INFO

Article history:
Received 25 September 2010
Revised 2 December 2010
Accepted 3 December 2010
Available online 9 December 2010

Keywords:
Antiviral drugs
HIV-1 reverse transcriptase
RNase H enzymatic activity
Inhibitors
Dual metal chelation
Nitro-furan carboxylic acid

ABSTRACT

Rapid emergence of drug-resistant variants is one of the most serious problems in chemotherapy for HIV-1 infectious diseases. Inhibitors acting on a target not addressed by approved drugs are of great importance to suppress drug-resistant viruses. HIV-1 reverse transcriptase has two enzymatic functions, DNA polymerase and RNase H activities. The RNase H activity is an attractive target for a new class of antiviral drugs. On the basis of the hit chemicals found in our previous screening with 20,000 small molecular-weight compounds, we synthesized derivatives of 5-nitro-furan-2-carboxylic acid. Inhibition of RNase H enzymatic activity was measured in a biochemical assay with real-time monitoring of florescence emission from the digested RNA substrate. Several derivatives showed higher inhibitory activities that those of the hit chemicals. Modulation of the 5-nitro-furan-2-carboxylic moiety resulted in a drastic decrease in inhibitory potency. In contrast, many derivatives with modulation of other parts retained inhibitory activities to varying degrees. These findings suggest the binding mode of active derivatives, in which three oxygen atoms aligned in a straight form at the nitro-furan moiety are coordinated to two divalent metal ions located at RNase H reaction site. Hence, the nitro-furan-carboxylic moiety is one of the critical scaffolds for RNase H inhibition. Of note, the RNase H inhibitory potency of a derivative was improved by 18-fold compared with that of the original hit compound, and no significant cytotoxicity was observed for most of the derivatives showing inhibitory activity. Since there is still much room for modification of the compounds at the part opposite the nitro-furan moiety, further chemical conversion will lead to improvement of compound potency and specificity.

1. Introduction

A cocktail regimen of therapeutic agents known as highly active antiretroviral therapy (HAART) showed a great advance in the treatment of human immunodeficiency virus (HIV) infectious diseases. The efficacy of this therapy is, however, limited by the emergence of drug-resistant variants of HIV-1. Drug-resistant viruses have become a serious issue in current HIV chemotherapy[1] because HIV-infected disease inevitably requires long-term treatment. One of the effective and practical measures to suppress drug resistance is to produce new anti-HIV drugs that act on the target not addressed by approved drugs. Drugs directly blocking the viral enzymatic activity usually show a high therapeutic performance. RNase H activity of reverse transcriptase (RT) is the enzymatic activity of HIV-1 that no approved drugs still act on. Since it is possible to take an inhibitor of RNase H activity with other approved drugs, the RNase H inhibition is expected to be one of the attractive targets for anti-HIV drugs.[2]

RT is a virally encoded enzyme of HIV-1. RT is a heterodimer of p51 and p66 subunits and has enzymatic functions of DNA polymerase and RNase H activity. That is, this enzyme converts single-strand viral genomic RNA into double-strand DNA. The enzyme also catalyzes the hydrolysis of RNA phosphodiester bonds of RNA hybridized to DNA. Two spacely-separated active sites with the same protein are responsible for these two enzymatic functions respectively. Hence, RT-associated RNase H activity is one of the attractive targets for developing a novel class of antiviral drugs. Furthermore, dual inhibitory of RNase H activity and the activity of RT-associated polymerase or HIV-1 integrase has been reported because of the structural similarity of their catalytic sites.[3–5]

RNase H activity requires the presence of divalent metal cations to be functionalized in catalysis of endo-nucleolytic phosphodiester hydrolysis. Recent crystallographic studies have shown the

* Corresponding author. Tel.: +81 43 290 2926; fax: +81 43 290 2925.
E-mail address: hoshino@faculty.chiba-u.jp (T. Hoshino).

0968-0896/$ - see front matter © 2010 Elsevier Ltd. All rights reserved.
doi:10.1016/j.bmc.2010.12.011

bimetal mode of divalent metal.[6–8] The enzymatic active site contains four carboxylate residues, creating an environment capable of stabilizing two metal ions. Many RNase H inhibitors are assumed to be bound to the catalytic center and interact with divalent metal ions. That is, chelators of these metal ions are regarded as potential inhibitors of the function of HIV-1 RNase H.

Several different scaffolds have been reported as inhibitors of RNase H activity.[9–13] Diketo acids have been well-known chemical structure showing potent inhibitory for two divalent metal-related enzymatic activity initiating endonucleolytic phosphodiester hydrolysis.[14] Therefore, diketo acid structure has served as a starting point for the design and optimization of inhibitors of HIV-1 integrase or influenza endonuclease. Pyrimidinol is one of typical derivatives bearing a scaffold called *N*-hydroxyimide,[15] and it has been reported to be a potent inhibitor of HIV-1 RNase H function, acting through metal chelation at the active site. *N*-hydroxyimides were firstly described as inhibitors of influenza endonuclease, but they also show high potency in biochemical assays of HIV-1 RNase H. An important feature in the structure of pyrimidinol is a six-member ring having a polar atom alignment compatible with diketo acids. The natural product β-thujaplicinol is another scaffold and has been reported to be a highly potent inhibitor of HIV-1 RNase H activity.[16] Using this chemical, the multiple inhibition of HIV-1 enzymes such as HIV-1 integrase and HIV-1 RT-associated polymerase has been investigated. The prominent feature in the structure of β-thujaplicinol is a seven-member ring bonding with two hydroxy groups and one carboxy group.

From an in vitro screening using 20,000 small molecular-weight compounds, we found chemicals that blocked HIV-1 RT-associated RNase H activity.[17] Several analogues bearing the 5-nitro-furan-2-carboxylic acid ester moiety were shown to work as retroviral RNase H inhibitors. Two of the derivatives were capable of suppressing HIV-1 replication in tissue culture. The distinguishable feature in the structure of our 5-nitro-furan-2-carboxylic acid ester is a five-member ring.

To date, no RNase H inhibitors have been approved for clinical use. One of the problems in developing an RNase H active site inhibitor is the absence of a deep pocket into which the inhibitors can be bound.[7,18] This makes it difficult to improve stable and specific binding of compounds to the RNase H catalytic site. Metal ions at the active site, however, are a suitable aiming point for inhibitor binding. A diketo acid inhibitor was shown to be bound in a metal-dependent manner to the RNase H domain of RT.[14,19] Pyrimidinol analogues were designed to chelate the divalent metals of the RNase H domain.[6] β-Thujaplicinol also chelates the two metal ions at the active site.[7] Judging from the structural similarity to pyrimidinol or β-thujaplicinol, derivatives bearing the 5-nitro-furan-2-carboxylic acid ester moiety are assumed to chelate two divalent metal ions as well.

In this study, we examined chemical compounds for anti-HIV drugs blocking RT-associated RNase H enzymatic activity. A variety of compounds were synthesized on the basis of hit chemicals found in in vitro screening in our previous study. Measurement of inhibitory activity with a fluorescence-based assay and theoretical calculation using quantum mechanical (QM) and molecular mechanics (MM) methods suggested the binding mode of the synthesized compounds. The findings of the present study provide a strategy for designing a chemical structure to enhance the inhibitory activity.

2. Methods

2.1. Organic synthesis

Derivatives from a hit compound bearing 5-nitro-furan-2-carboxylic acid were synthesized to obtain chemical analogs showing high inhibitory activity for RNase H. Parts A, B and C of the hit compound shown in Figure 1a were converted into other chemical substitutes. Then compounds **1–53** were synthesized according to the routes shown in the scheme of Figure 1b.

First, chemical modulation was performed for part A. Part A is composed of large hydrophobic substitutes. Compounds **1–28** were prepared by nucleophilic substitution reaction of 5-nitro-2-furoic acid with an α-chloro carbonylate in the presence of DMAP in DMF at 80 °C (eq. 1 of Fig. 1b). Second, chemical modulation was performed for part B, which shows a large hydrophilicity with a nitro-furan moiety. Compounds **29–45** were prepared by experimental conditions similar to those used in the reaction for converting part A. A substitution reaction was carried out using carboxylic acids that contain a nitro group on the aromatic ring (eq. 2 of Fig. 1b). Third, the chemical structure of part C was modulated. Part C is a region connecting parts A and B. 5-Nitro-2-furoic acid was treated with thionyl chloride to generate an acid chloride as an intermediate, followed by reaction of the generated acid chloride with an α-amino acid ester to produce compounds **46–51** (eq. 3 of Fig. 1b). Additionally, two compounds **52** and **53** were prepared to modulate parts A and C with keeping the ester bond. 5-Nitro-2-furoic acid was converted into an acid chloride as an intermediate with thionyl chloride, followed by the substitution reaction of nucleophilic reagents (eq. 4 of Fig. 1b).

2.2. Evaluation of inhibitory activity

Plasmids expressing p66 or p51 of RT with a hexahistidine tag were prepared by cloning a DNA fragment encoding the HIV-1 RT into the pQE-9 vector.[17] The *Escherichia coli* strain BL21(DE3)pLysS was transformed with the plasmids, and protein expression was induced by treatment with 1 mM isopropyl β-D-thiogalactoside for 3 h. For generating heterodimers, bacteria lysates expressing p66 and p51 were mixed prior to purification. A gradient elution was performed using HiTrap HP columns according to the manufacturer's protocol. The yield of the purified protein was estimated using bovine serum albumin as a standard, and the purification was evaluated with Coomassie blue-stained SDS–polyacrylamide gels. The concentration of HIV-1 RT was approximately 1×10^4 units/g, which was determined by a comparison of polymerase activity with an RT standard.[17]

Alternatively, the expression plasmid vector RT69A, which was kindly provided by Professor E. Arnold at Rutsgers University, was used. This plasmid expresses a heterodimer of p66 and p51, which was reported to produce RT crystals with a resolution below 2 Å in X-ray diffraction analysis due to amino residue mutations of F160S and C280S.[20] The *E. coli* strain Rosetta transformed with the RT69 plasmid was incubated at 37 °C. Protein expression was induced by adding 1 mM isopropyl β-D-thiogalactoside at an OD_{600} value of 0.9 and completed by incubation for 3 h after induction. A cell pellet corresponding to 1.5 L of culture was resuspended in 50 mM Tris–HCl at pH 8.0, 600 mM NaCl, and 1% Triton X-114. The bacterial cell membrane was disrupted by sonication. After removing unnecessary disrupted fragments from the lysate by centrifugation, the expressed protein was obtained from the supernant. Since the RT p51 subunit contains an N-terminal hexahistidine tag, RT was purified by using a HiTrap Ni affinity column with an elution buffer containing 500 mM imidazole. The eluted protein fraction was dialyzed overnight against a buffer containing 50 mM Tris–HCl at pH 8.0 and 600 mM NaCl. The dialyzed RT was incubated with HRV 3C protease for 24 h at 4 °C to cleave the hexahistidine tag attached to the N-terminus of the p51 subunit of the heterodimer RT protein. The protein was again purified by Ni-NTA according to the manufacturer's recommendation to remove the uncleaved protein and HRV 3C protease. The RT69 protein was dia-

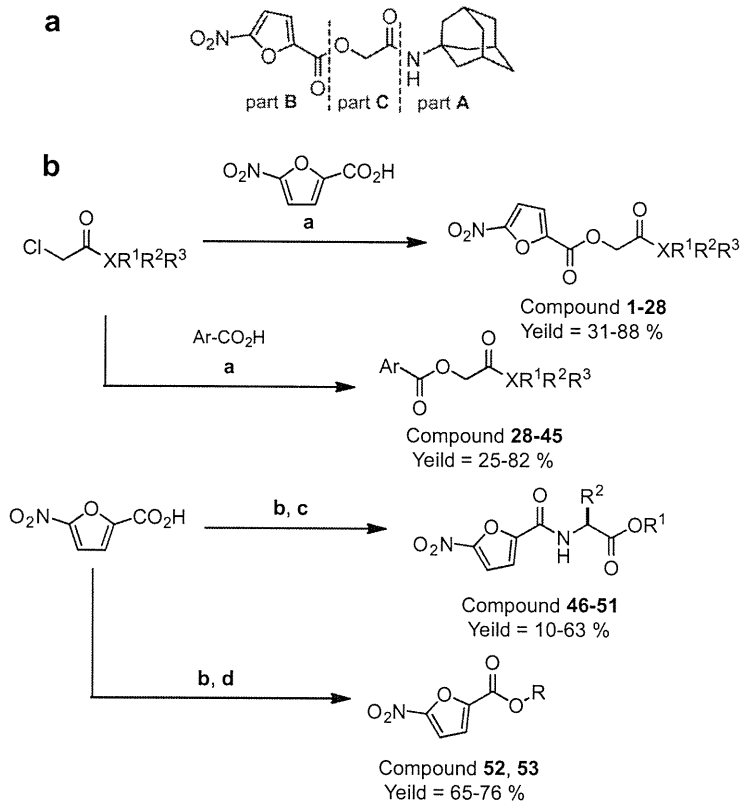

Figure 1. (a) Structure of a hit chemical showing RNase H inhibitory activity found in our previous in vitro screening. (b) Scheme for synthesis of the derivatives from the hit chemical. Eqs. 1, 2 and 3 correspond to the reactions for modulating parts A, B and C in (a), respectively. Eq. 4 indicates the reaction modulating the moiety connected to the ester bond at parts A and C.

lyzed against a buffer of 50 mM Tris–HCl at pH 7.5 and 200 mM NaCl and was stored at −20 °C with adding 50% (v/v) glycerol.

The inhibitory activities of synthesized compounds were measured by an enzymatic assay in a manner similar to that in the previous studies.[17,21,22] In short, a real-time monitoring assay was applied. For substrate, two oligo-nucleotides were annealed at final concentrations of 2.5 and 0.25 μM. One was oligo-ribonucleotide 5′-GAUCUGAGCCUGGGAGCU-3′ with 6-carboxy-fluoroscein (FAM) conjugated at the 3′ end, and the other was oligo-deoxyribonucleotide 5′-AGCTCCCAGGCTCAGATC-3′ with black hole quencher (BHQ) conjugated at the 5′ end. Enzyme reaction with 100 ng RT, 0.025 μM oligo-ribonucleotide, and 0.25 μM oligo-deoxyribonucleotide was carried out in a volume of 10 μL at 37 °C. Fluorescence at 488 nm was monitored every 150 s using a multimode detector.

2.3. Assessment of cytotoxicity

Cytotoxicity of the synthesized compounds was tested by an MTT assay with the celltiter 96 non-radioactive cell proliferation assay system (Promega). Two cell lines, MT-4 and 293T, were used in this assay. The cytotoxic assay was performed by the following 8-step procedure. (1) 100 μL RPM-1640 medium supplemented with 10% FBS containing 2% DMSO was loaded in a 96-well plate, and the outside of the wells was soaked with 100 μL PBS to prevent an edge effect. (2) 200 μL RPM-1640 medium with 10% PBS and 2% DMSO containing test compounds at a concentration of 200 μM was added to the wells in the first column of the plate. The final concentration of the compounds in these wells was 100 μM when cells were cultured. (3) A sequence of wells with different compound concentrations was prepared for the second, third and fourth columns. The final concentrations of these columns were 50, 25 and 12.5 μM. The wells in the fifth column were used for a control without adding any test compounds. (4) 100 μL MT-4 cells at a concentration of 4×10^5/mL or 100 μL 293T cells at a concentration of 2×10^5/mL was added to the respective wells. The final concentration of DMSO in each well was 1%. (5) Cells were incubated for 3 days at 37 °C with 5% CO_2 atmosphere. (6) 100 μL of supernant of the cultured medium was removed. Then 15 μL MTT reagent for dye solution was added to each well and the cells were incubated for 1 h. (7) 100 μL solution of solubilization and stop mix was added, and the cells were incubated overnight at 4 °C to sufficiently dissolve the dye. (8) Intensity of $OD_{570/690}$ was measured by a spectrofluorometer, BIO-TEK ELx808. Drug concentration showing 50% cell cytotoxicity was calculated only if the viability of cells was below 50% in the presence of compound at 100 μM.

2.4. Theoretical computation

A computational model of the target protein was constructed from an X-ray crystal structure of the RNase H domain of HIV-1 RT: 3HYF.[6] According to the results of the recent X-ray crystallographic studies on the complex of RNase H domain and chemical compounds showing RNase H inhibitory activity,[6–8] the RNase H

domain contains two Mn^{2+} ions at the center of the active site. Hence, two Mn^{2+} ions in the crystal structure were replaced with Mg^{2+} ions. The protonation states of all the ionasable residues were predicted by ProPKa program[23] in the presence of two Mg^{2+} ions at the active site. The prediction indicated deprotonation of Asp443, Glu478, Asp498, and Asp549. Chemical structures of the active compounds were built by using GaussView software, and geometry optimization was executed at the B3LYP/6-31G(d,p) level. Each compound was manually placed at the active site of RNase H domain. A quantum mechanical and molecular mechanics (QM/MM) approach was applied,[24] utilizing the ONIOM method of GAUSSIAN 03 program.[25] In our preliminary computations, molecular dynamics simulation hardly gave a reasonable binding conformation, because the RNase H domain contained divalent metal ions at the active site and the parameterization would be insufficient to reproduce the six-fold coordination of divalent metal ions. In QM/MM calculation, Asp443, Glu478, Asp498, Asp549, His539, compound, and two Mg^{2+} ions were set to the QM layer, and the other residues were set to the MM layer. No water molecules were included in the calculation model. Models including surrounding water molecules had also been examined in our preliminary trials of QM/MM calculation. Geometry optimization was hardly completed in the water-included models because of the difficulty in meeting the convergence criteria, in which even slight forces on atoms caused large displacements of the surrounding water molecules. Molecular orbitals in the QM layer were calculated at the B3LYP/6-31G(d,p) level and the universal force field was applied to the atoms in the MM layer. Geometry optimization was executed without any constraints to any atoms.

3. Results

Two hit chemicals, which were found in our previous in vitro screening, contain a nitro-furan ring and amide group bonding to

Table 1
Structure and RNase H inhibitory activity of the derivatives modulated at part A

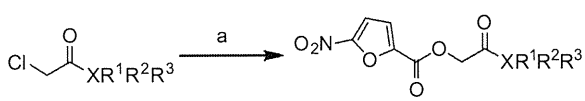

Compound **1-28**
Yeild = 31-88%

Conditions ; (a) 5-Nitro-2-furoic acid, DMAP, DMF, 80 °C, 6 h

Compound	X	R^1, R^2, R^3	Yield (%)	IC_{50} (μM)
1	O	R^1 = *i*-Pr	64	13.2
2	N	R^1 = H, R^2 = *t*-Bu	58	18.0
3		R^1 = H, R^2 = CMe_2Et	48	5.8
4		R^1 = H, R^2 = CMe_2Ph	43	8.2
5		R^1 = H, R^2 = CMe_2CH_2Ph	48	4.3
6		$R^1 = H, R^2 = CH_2\overline{CH(CH_2)_3O}$	64	4.2
7		R^1 = H, R^2 = 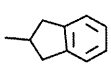	59	5.5
8	N	R^1 = H, R^2 = 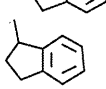	38	6.1
9		R^1 = H, R^2 = 	45	4.3
10	N	R^1 = *t*-Bu, R^2 = CH_2Ph	82	0.9
11		R^1 = *t*-Bu, R^2 = CH_2CH_2Ph	74	14.2
12		R^1 = *t*-Bu, R^2 = $CH_2(CH_2)_2Ph$	82	>50
13		R^1 = *t*-Bu, R^2 = $CH_2CH_2C(O)Ph$	88	>50
14	N	R^1 = *t*-Bu, R^2 = CH_2*p*-$NO_2C_6H_4$	72	6.9
15		R^1 = *t*-Bu, R^2 = CH_2*m*-$NO_2C_6H_4$	69	9.8
16		R^1 = *t*-Bu, R^2 = CH_2*p*-$AcOC_6H_4$	45	8.7
17		R^1 = *t*-Bu, R^2 = CH_2*o*-$AcOC_6H_4$	31	12.8
18		R^1 = *t*-Bu, R^2 = CH_2*p*-$MeOC_6H_4$	68	7.5
19		R^1 = *t*-Bu, R^2 = CH_2*p*-$BnOC_6H_4$	73	>50
20	N	R^1 = *t*-Bu, R^2 = CH_2*p*-FC_6H_4	64	8.5
21		R^1 = *t*-Bu, R^2 = CH_2*p*-$CF_3C_6H_4$	71	8.0
22		R^1 = *t*-Bu, R^2 = CH_2*m*-$CF_3C_6H_4$	69	8.5
23		R^1 = *t*-Bu, R^2 = CH_2*o*-$CF_3C_6H_4$	72	9.0
24		R^1 = *t*-Bu, R^2 = $CH_2$2,3,4,5,6-F_5C_6	68	6.8
25	N	$R^1 = CH_2\overline{CH(CH_2)_3O}$, $R^2 = CH_2Ph$	32	7.7
26		$R^1 = CH_2\overline{CH(CH_2)_3O}$, $R^2 = CH_2$*p*-HOC_6H_4	45	5.0
27	C	R^1 = H, R^2 = H, R^3 = H	56	7.1
28		R^1 = Me, R^2 = Me, R^3 = Me	49	21.9

Conditions: (a) 5-nitro-2-furoic acid, DMAP, DMF, 80 °C, 6 h.